THE GEOLOGICAL SOCIETY OF AMERICA®

Evolution of fluvial meander-belt deposits and implications for the completeness of the stratigraphic record

Paul R. Durkin[1,†], Stephen M. Hubbard[1], John Holbrook[2], and Ron Boyd[3]
[1]*Department of Geoscience, University of Calgary, 2500 University Drive NW, Calgary, Alberta T2N 1N4, Canada*
[2]*Department of Geology, Texas Christian University, Fort Worth, Texas 76129, USA*
[3]*School of Environmental and Life Sciences, University of Newcastle, Callaghan, NSW 2308, Australia*

ABSTRACT

The fragmentary nature of the stratigraphic record is particularly evident with respect to fluvial deposits, which are characterized by a hierarchy of depositional units deposited over a wide range of time scales and sedimentation rates. We quantified stratigraphic completeness in meander-belt deposits through deducing the total area of bar sedimentation versus what is ultimately preserved in the depositional record, using area as a surrogate metric for sediment volume. Data sets were evaluated for a numerical model, the modern Mississippi River valley, and the Cretaceous McMurray Formation. In each data set, the evolutionary history of a series of meander-belt elements was discerned. Migrated area between successive reconstructed paleochannel positions was measured, representing: total area of net bar migration (MA), the area of bar preserved (PA), and percent of bar preserved (PA/MA), at the accretion package, bar, and meander-belt scale.

Results of our analysis show that the average preservation percent ranges from 27.3% to 67.8% for an accretion package, 35.0% to 85.1% for a bar, and 38.2% to 67.6% for a meander belt. The processes that lead to a decrease in preservation include intra-meander-bend erosion (due to downstream translation or bar rotation), and increasing meander-bend sinuosity and eventual cutoff (neck and chute), as well as inter-meander-bend erosion due to avulsion and subsequent migration of the meandering channel. The results of this study document a decrease in preservation over time that follows a natural logarithmic function of decay; we have termed this the "survivability" curve. The results presented here document a systematic, monotonic decrease in preservation over time, which is consistent regardless of the spatial or temporal scale and agrees with probabilities of preservation at long time scales proposed by previous workers. A comparison between data sets allows for an estimation of the time span represented by meander-belt deposits in the deep time record.

INTRODUCTION

Investigation and interpretation of the stratigraphic record are understandably biased toward what is preserved, rather than gaps of missing time not directly represented. In his formative *GSA Bulletin* contribution 100 yr ago, Barrell (1917, p. 797) proposed that only "one sixth of time is recorded" in the stratigraphic record. Unravelling information about gaps in the rock record represents a significant opportunity to enhance interpretations of deep-time depositional settings and sedimentary processes.

Sadler (1981) showed that rates of sediment accumulation are inversely related to the time scale over which they are measured. This concept is commonly referred to as the "Sadler effect." The results of Sadler's synthesis reveal the impact of increasing the number and duration of intervals of stasis or erosion as the window of observation increases (Miall, 2014a), resulting in an apparent decrease in sediment accumulation rates with time. Following this, Sadler and Strauss (1990) defined the concept of stratigraphic completeness in order to evaluate the amount of time that has been recorded in a stratigraphic section. The completeness of a stratigraphic section is defined as "the fraction of time intervals of some specified length (*t*) that have left a record" (Sadler and Strauss, 1990, p. 471; Fig. 1 herein). Sadler's (1981) initial investigation used net sediment accumulation as the dependent variable, which captures the three factors that control completeness: deposition, stasis, and erosion. The most important factor for completeness, however, is leaving a record (i.e. preservation); a record consists of sediment deposited over *t* that is not subsequently eroded (Sadler and Strauss, 1990; Fig. 1 herein).

The frequency and magnitude of deposit erosion (or preservation) at the scale of a sedimentary body have received relatively little attention in the context of stratigraphic completeness (e.g., Trabucho-Alexandre, 2014; Mahon et al., 2015). Theoretical models of the unsteadiness of sedimentation over time, generated from calculated average sedimentation rates for *t*, inherently capture erosion of sedimentary bodies through the use of average sedimentation rates as the dependent variable (Sadler, 1981; Strauss and Sadler, 1989; Sadler and Strauss, 1990; Miall, 2014a). However, those sedimentary bodies are often scaled to that given time scale *t* (Sadler, 1981; Sadler and Strauss, 1990; Schumer and Jerolmack, 2009; Miall, 2014a). It is the removal of those deposits during time scales longer than that of the original *t* that is captured by lower net sediment accumulation rates over longer time intervals. Sadler and Strauss (1990) showed that as time increases, the likelihood for preservation of a sedimentary package decreases (Fig. 2). Therefore, we aimed to document the decrease in preservation percentage of a sedimentary body over time to inform understanding of the processes responsible for the observed decreasing average sediment accumulation rates over time ("Sadler effect").

Current understanding of the rates of sedimentary body decay relies on continuous observation of deposition and erosion (e.g., Fig. 1). Specific case studies that document stratigraphic completeness are relatively uncommon (e.g., Wetzel and Aigner, 1986; Prokoph and Agterberg, 1999; Lewin and Macklin, 2003; Lowenstein et al., 2003; Sommerfield, 2006; Straub and Esposito, 2013; Miall, 2014b; Trabucho-Alexandre, 2014; Mahon et al., 2015)

†Present address: Department of Geological Sciences, University of Manitoba, 66 Chancellors Circle, Winnipeg, Manitoba R3T 2N2, Canada; paul.durkin@umanitoba.ca.

GSA Bulletin; May/June 2018; v. 130; no. 5/6; p. 721–739; https://doi.org/10.1130/B31699.1; 15 figures; 2 tables; Data Repository item 2017379; published online 20 December 2017.

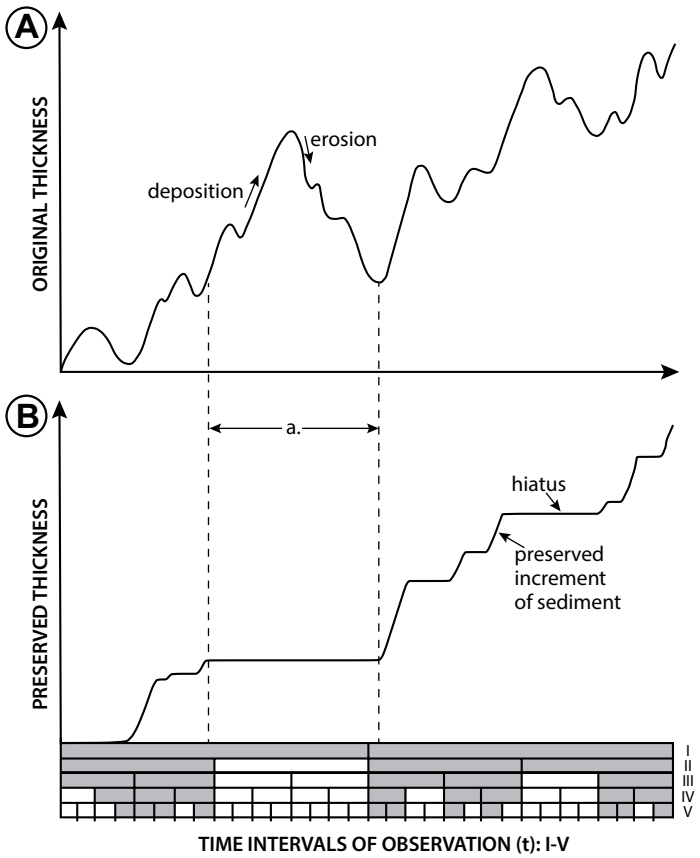

Figure 1. The concept of stratigraphic completeness (modified from Sadler and Strauss, 1990). (A) A time series of sediment thickness determined by continuous monitoring of a hypothetical stratigraphic section. Sediment deposition occurs when the graph is increasing, and erosion occurs when it is decreasing. (B) A "staircase" plot for the same section as A, which contains information on preservation and thickness that can only be gleaned from the stratigraphic section itself. The *x*-axis for both A and B represents five time intervals of observation (I–V), where shaded time intervals have left a record. For example, all of the deposition that occurs in time span "a" is eroded during the same time span; therefore, (1) the preserved thickness remains constant (hiatus), and (2) time scales "II–V" are not shaded because no record has been left during those time intervals (*t*). Completeness is defined as the number of time intervals (*t*) that have left a record (Sadler and Strauss, 1990). When considering the entire graph, time scale I is fully complete because a record was preserved during both time intervals, whereas time scale V has a completeness of 0.34 because, of the 32 time intervals, only 11 have left a record (11/32 = 0.34).

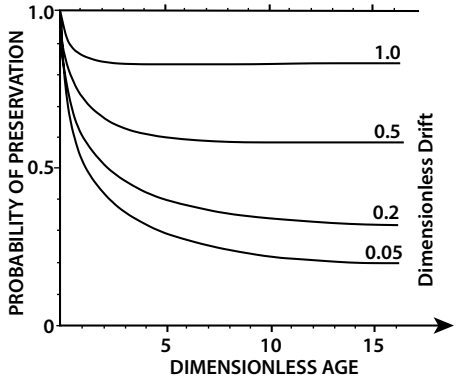

Figure 2. Theoretical model of stratigraphic completeness for a stratigraphic section (after Sadler and Strauss, 1990). Graph shows the probability of preservation, which is a function of dimensionless age (*x*-axis) and dimensionless drift (family of curves). Dimensionless drift refers to net long-term accumulation rate. Each curve levels out at a constant probability at large values of dimensionless age. Therefore, for a long section, the expected completeness becomes the same as the constant probability of preservation and depends solely on dimensionless drift.

due, in part, to the limited time scale over which humans can observe sedimentary processes, a lack of sufficient dating capabilities, and the inherent difficulty of interpreting what is not preserved. The fragmentary nature of the stratigraphic record has been considered with respect to fluvial deposits, which are characterized by a hierarchy of units associated with deposition over a wide range of time scales and sedimentation rates (e.g., Miall, 1985; Sadler, 1981; Holbrook, 2001; Miall, 2014a, 2014b; Reesink et al., 2015). Observations of point bar growth in modern stream systems on annual to seasonal time frames, for example, have been made (e.g., Leopold and Wolman, 1960; Moody and Meade, 2014); however, these investigations have not captured erosional events that exist in meander belts over longer time intervals (Macklin et al., 2006; Fuller, 2008). Likewise, tracking the yearly migration of a meandering channel in successive satellite images (Fig. 3) does not typically capture erosional events with recurrence intervals >100 yr (e.g., Syvitski and Brakenridge, 2013). Therefore, if observation of modern sedimentary processes is insufficient to predict stratigraphic preservation, perhaps answers lie in more careful interpretations of the rock record.

The objectives of this study were to reconstruct fluvial channel migration patterns and interpret the evolution of a complex amalgam of bar and abandoned channel deposits preserved in deep-time strata. We hypothesized that the completeness of a depositional system can be quantified through paleochannel migration history analysis, by calculating the ratio of sediment deposited to sediment preserved in the rock record. In order to test this, we considered a series of meander belts spanning a wide range of spatial and temporal scales, including modern and recent deposits, and a numerical model, to inform our analysis of deep-time deposits. The completeness of the stratigraphic record was assessed in planform at the scale of accretion packages, bars, and meander belts (Fig. 4), using net migrated area as a surrogate metric for sediment volume. We focused on the decrease in preservation over time for a given sedimentary body (e.g., point bar deposit). The results inform more resolved paleoenvironmental interpretations, including estimates for the duration of ancient meander belts.

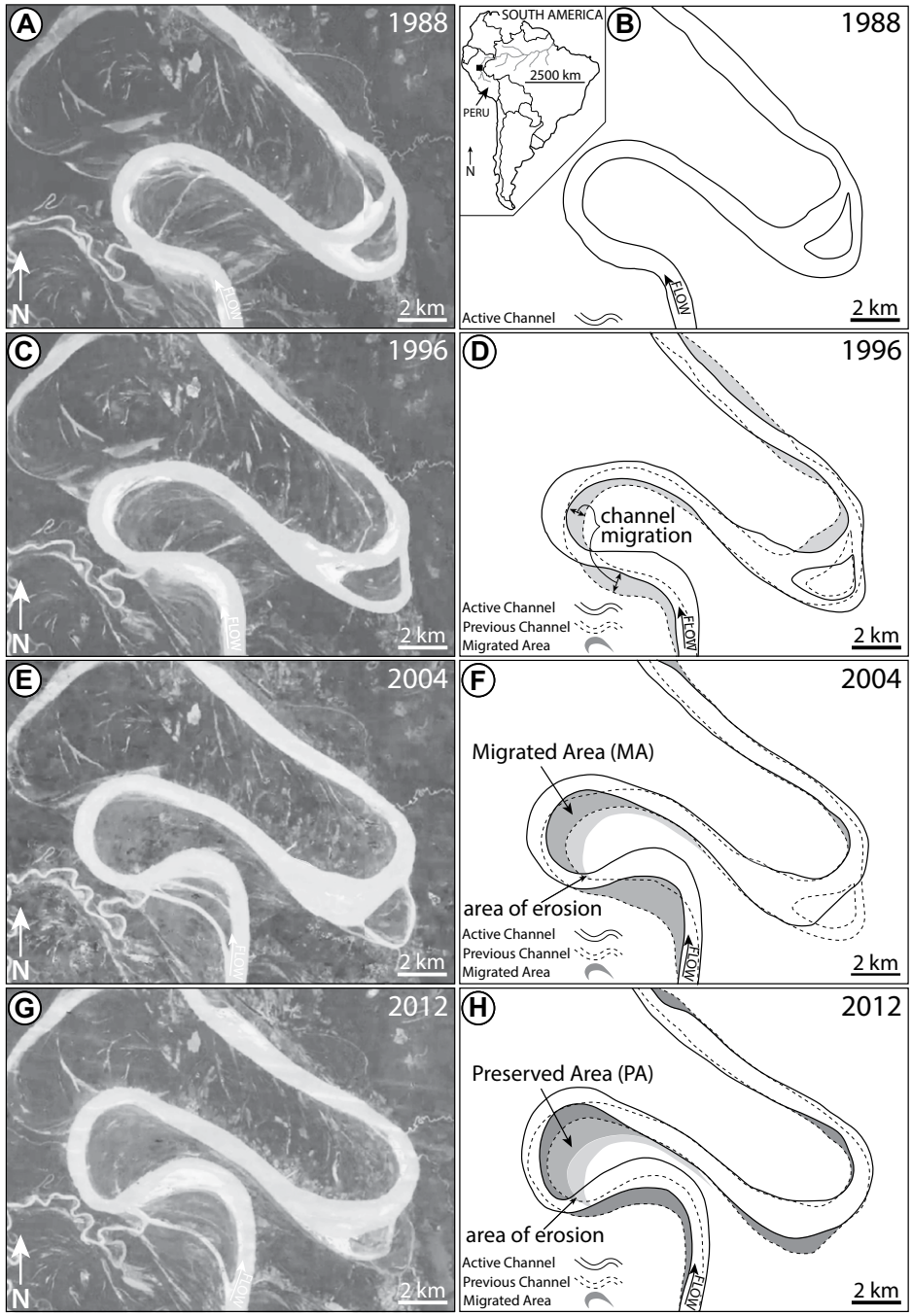

Figure 3. Satellite images of the Ucayali River, Peru (Lat: 7°38′32.17″S, Long: 75°0′48.85″W). Inset map indicates location in South America. (A, C, E, G) Satellite images showing changes in channel location every 8 yr. (B, D, F, H) Line tracings of the active channel (solid), previous channel (dashed), and migrated area (polygon) for each image on the left. Note that this meandering channel is situated on a megafan rather than a confined meander-belt valley. Nevertheless, it is a useful example to illustrate meander migration through time, applicable to the analyses undertaken in this study.

STUDY AREAS AND DATA

Our data set includes the results of a numerical model (NAYS2D; van de Lageweg et al., 2016), the modern and recent lower Mississippi River (New Madrid, Missouri, and Helena, Arkansas, United States), and a subsurface Lower Cretaceous meander belt (Aptian McMurray Formation, Alberta, Canada).

Numerical Model

A recent study by van de Lageweg et al. (2016) documented the preservation of meandering channel stratigraphy using a numerical model "NAYS2D" (Fig. 5). Model parameters, such as discharge, grain size, valley gradient, and morphological behavior, were drawn from the modern Rhine and Mississippi Rivers (Fisk, 1944; Hudson and Kesel, 2000; Stouthamer and Berendsen, 2000; Kleinhans and van den Berg, 2011). The model domain is 3 km wide and 10 km long with a gradient of 2.1×10^{-4} m/m and a grid cell size of 20 × 20 m (van de Lageweg et al., 2016). The channel begins as a straight 200-m-wide channel with a constant discharge of 2500 m^3/s and a uniform grain size of 2 mm. Each time step represents ~2 yr of meander migration, and our analysis focused from time steps $t = 293$ to $t = 668$ (van de Lageweg et al., 2016).

The resulting alluvial topography at time step $t = 668$ is characterized by a 9-km-long and up to 2.5-km-wide meander-belt deposit, with a high-sinuosity (2.37) meandering channel. The entire meander belt is composed of 14 convex point bars, 5 concave counter point bars, and 4 distinct abandoned channel (oxbow lake) fills. The point bars range from 0.5 to 2 km long and >1 km wide, and the abandoned channel fills are ~150 m wide. The meander bends associated with point-bar deposition are commonly simple symmetrical features, with simple asymmetrical and compound asymmetrical examples as well (Brice, 1974). The thickness of the deposit from cross-sectional data is ~20 m (van de Lageweg et al., 2016). We utilized an iteration of the model with no vertical aggradation component in order to enable realistic comparisons to other meander belts studied, and we did not use results beyond $t = 668$ due to instability that developed in the planform development after this point (van de Lageweg et al., 2016).

Lower Mississippi River

The Mississippi River is ~3900 km long, with a continental-scale drainage area of 3.2×10^6 km^2, including a vast expanse of the central United States to the Gulf of Mexico (Fig. 6A; Hudson and Kesel, 2000). The lower Mississippi River includes the 1700 km segment downstream of the confluence with the Ohio River at Cairo, Illinois (Fig. 6A). Two lower Mississippi River meander-belt segments were considered (Fig. 6A).

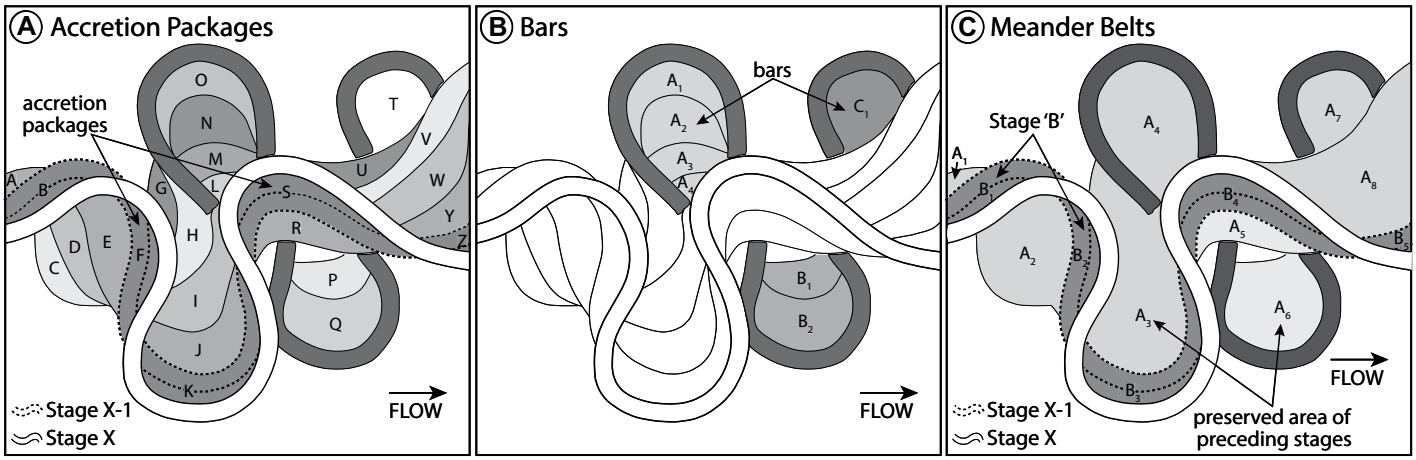

Figure 4. Definition and scale of features examined in this study. (A) Accretion packages are mapped as the net migrated area from the inner bank of stage X-1 (dashed line) to inner bank of stage X (solid line). Each letter represents one accretion package (25 total in this example). (B) Bars are mapped as the entire net migrated area up to the point where the meander loop reaches cutoff. Only bars associated with meander loops that reached the point of cutoff were measured. Bars are typically composed of several accretion packages (i.e., $A_1 + A_2 + A_3 + A_4$). In total, three bars are present in this example. (C) Meander belts are mapped as the net migrated area from stage X-1 to stage X along all meander bends, plus the preserved area of the preceding stages. For example, meander belt B = $(B_1 + B_2 + B_3 + B_4 + B_5) + (A_1 + A_2 + A_3 + A_4 + A_5 + A_6 + A_7 + A_8)$. The "$A_X$" polygons represent the preserved area of all preceding stages. Although this definition of "meander belt" is not consistent with other published definitions (e.g., Fernandes et al., 2016), it provides a relatively straightforward and effective parameter to measure for our analysis.

New Madrid, Missouri

The first Mississippi River study area is from Holbrook et al. (2006), which covers a 1670 km^2 area at New Madrid, Missouri (Fig. 6B). Holbrook et al. (2006) dated scroll bars and abandoned channel fills using optically stimulated luminescence (OSL) and radiocarbon (RC) dating techniques, respectively (Fig. 6C; Table 1). In addition to the dates and maps from that study, recent satellite images aided in the characterization of the meander belt at this location. Over the last ~8000 yr or more, the river has freely meandered within a 60-km-long and 30-km-wide valley that is partially confined by highlands to the east (Fig. 6B; Holbrook et al., 2006). The meander plain is characterized by a complex amalgam of point bars, counter point bars, and abandoned channel fills with a modern river sinuosity of 1.80. The point bars range in size from 2 to 15 km long and up to 10 km wide, and the abandoned channel fills range from 600 to 1800 m wide. The relatively narrow nature of the meander belt at this location has resulted in a high degree of reworking of older deposits, leaving small fragments of bars and abandoned channel fills preserved on the floodplain. The ages of each cycle of meander belt evolution have been constrained and serve as a basis for more detailed reconstructions at a finer temporal resolution (Holbrook et al., 2006; Fig. 6C).

Helena, Arkansas

The second Mississippi River location is an ~485 km^2 area located approximately ~25 km upstream of the confluence with the St. Francis River at Helena, Arkansas (Fig. 6A). Satellite images and maps from Fisk (1944) were used to document meander-belt characteristics. The meander belt is 29 km long and up to 22 km wide, across which the river has freely meandered over the last several thousand years (Fig. 6E; Fisk, 1944). The meander plain is characterized by 16 point bars, 3 counter point bars, and 9 distinct abandoned channel (oxbow lake) fills. The point bars range from 2 to 6 km long and 2 to 4 km wide, and the abandoned channel fills range from 700 to 1600 m wide. The modern river exhibits a sinuosity of 1.52, and meander bends associated with point bar deposition are commonly simple symmetrical features, with simple asymmetrical and compound asymmetrical examples present as well (Brice, 1974). A factor of note, the thickness and lithology of the meander-belt deposits are not constrained in either the Mississippi River data set or along the entire lower Mississippi Valley, where the morphology of the river has been anthropogenically influenced over the last ~100 yr (Hudson and Kesel, 2000).

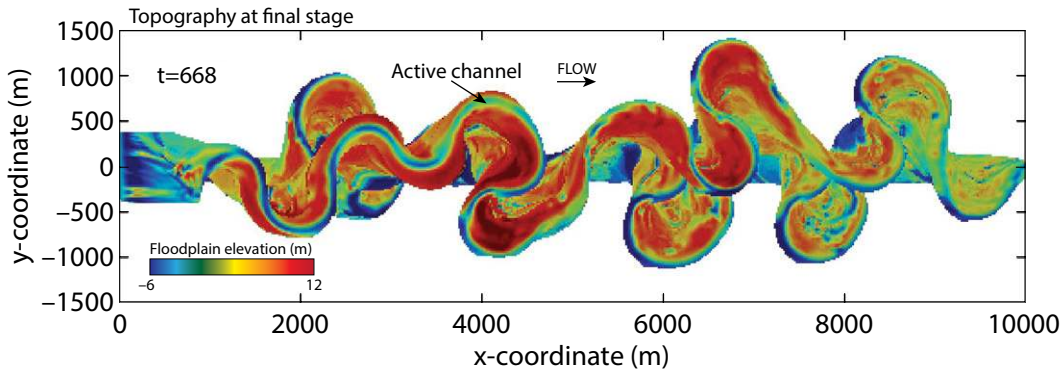

Figure 5. NAYS2D numerical model of meandering channels (modified from van de Lageweg, 2016). Planform topographic map of the final stage of evolution (t = 668) is characterized by a sinuous channel, point bars, counter point bars, and abandoned channels.

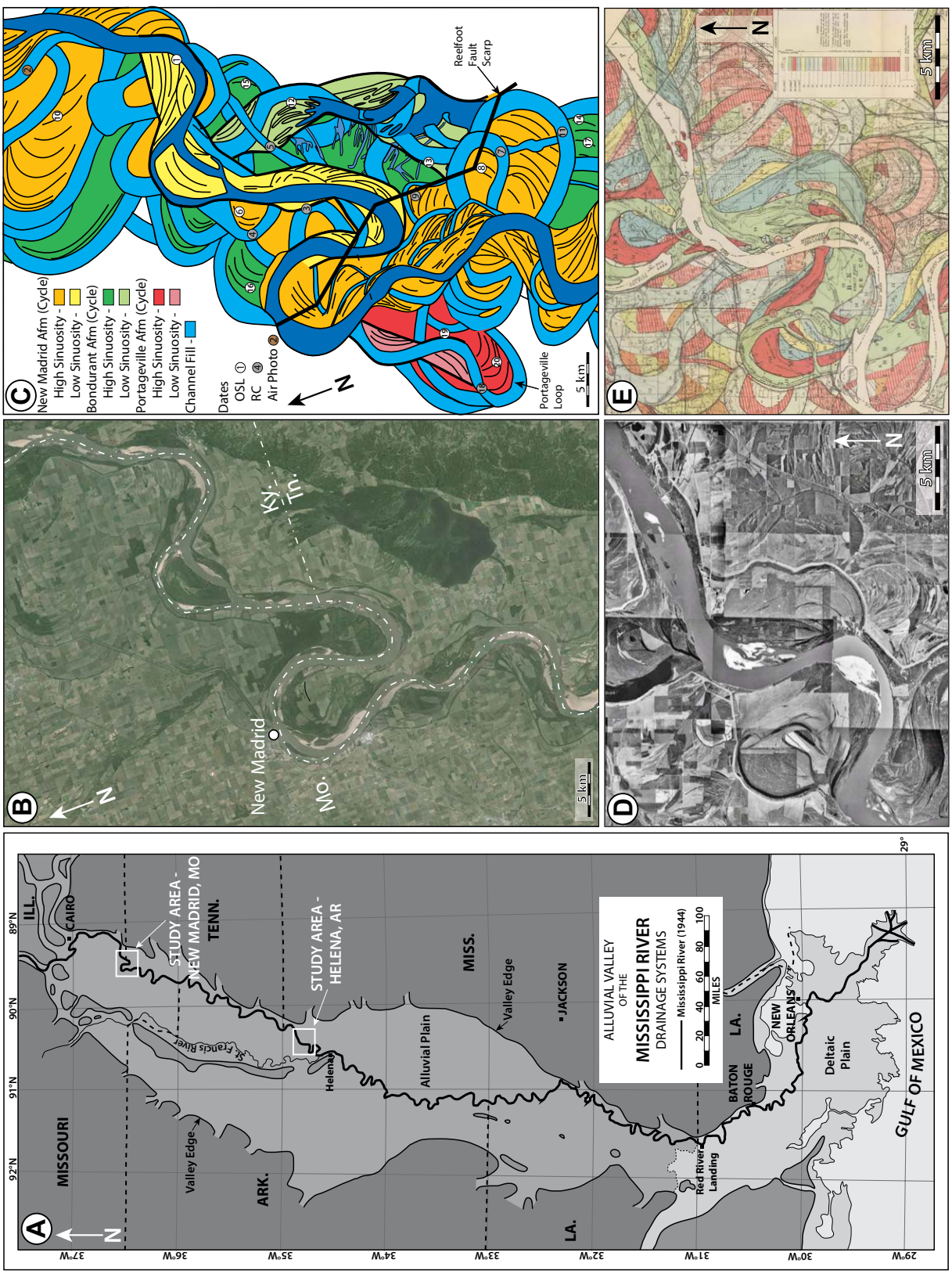

Figure 6. Study area locations. (A) Lower Mississippi River drainage system and channel location from 1944, indicating New Madrid, Missouri (MO), and Helena, Arkansas (AR), study areas (modified from Fisk, 1944). State abbreviations: Ill.—Illinois, Tenn.—Tennessee, Ark.—Arkansas, Miss.—Mississippi, LA.—Louisiana. (B) Satellite image of the modern Mississippi River and associated floodplain at New Madrid, Missouri. State abbreviations: Ky—Kentucky, Mo—Missouri, Tn—Tennessee. (C) Meander-belt interpretation from Holbrook et al. (2006), including location and method of dating samples (OSL—optically stimulated luminescence; RC—radiocarbon, Afm—alloformation). (D) Satellite image of the modern Mississippi River and associated floodplain north of Helena, Arkansas. (E) Map of segmented reconstructed channels from Fisk (1944).

TABLE 1. NEW MADRID SEISMIC ZONE OPTICALLY STIMULATED LUMINESCENCE (OSL) AND RADIOCARBON (RC) DATES

Point number	Location	Date type	Age	Date (yr B.P., relative to 2015)	Error
1	New Dorena loop	OSL	Modern	0	N/A
2	Wolf Island loop	Air photo	A.D. 1792	223	N/A
3	Donaldson loop	RC	A.D. 1213	801	+175/–66
4	Hubbard Lake loop	RC	A.D. 1167	848	+128/–89
5	Willow Pond chute cutoff	RC	A.D. 980	1035	+87/–37
6	Hubbard Lake scroll	OSL	A.D. 750	1265	+70/–70
7	Tiptonville loop	RC	B.C. 273	2288	+114/–69
8	Tiptonville scroll	OSL	B.C. 300	2315	+220/–220
9	Chrononville loop	RC	B.C. 475–200	2215–2490	
10	Towosahgy loop	OSL	B.C. 490	2505	+180/–180
11	Isom loop	RC	B.C. 798	2813	+35/–234
12	Bondurant loop	OSL	B.C. 1304	3319	+306/–306
13	Needle Eye loop	OSL	B.C. 1620	3635	+220/–220
14	Ridgely loop	OSL	B.C. 1680	3695	+270/–270
15	Hamby loop	OSL	B.C. 2244	4259	+269/–269
16	St. John's loop	OSL	B.C. 2590	4605	+230/–230
17	Ridgely loop	OSL	B.C. 2720	4735	+300/–300
18	Portageville Late Stage channel	RC	B.C. 4292	6307	+65/–245
19	Point Pleasant loop	OSL	B.C. 5250	7265	+360/–360
20	Portageville loop	OSL	B.C. 5484	7499	+376/–376

Early Cretaceous McMurray Formation

A subsurface meander belt in Lower Cretaceous strata (Aptian McMurray Formation) in northeastern Alberta, Canada, is revealed in high-quality three-dimensional (3-D) seismic-reflection data along a >100 km north-south–oriented transect (Fig. 7A; e.g., Smith et al., 2009; Hubbard et al., 2011; Labrecque et al., 2011; Musial et al., 2012; Durkin et al., 2017). The meander-belt deposits are located ~70 km southeast of Fort McMurray, Alberta, Canada, and the data set consists of ~400 km^2 of high-quality 3-D seismic data and a dense 3-D grid of data from oil well penetrations spaced ~500–1000 m apart (Fig. 7). Based on seismic geomorphologic and detrital zircon data, Musial et al. (2012), Benyon et al. (2014), and Blum and Pecha (2014) suggested that the catchment for McMurray Formation river sediments was potentially of continental scale, comparable to that of the modern Mississippi River.

Using seismic and well-bore data, series of observations were made to define a study area that is characterized by a 32-km-long and up to 21-km-wide ancient meander-belt deposit (Fig. 7C; Durkin et al., 2017). Scroll bar topography was not observed in the subsurface data; instead, channel migration patterns were deduced from the lithologic contrast between dipping lateral accretion layers (e.g., Hubbard et al., 2011). The interbedded lithology was validated by gamma-ray borehole logs (Fig. 7B). Seventeen bars were identified, including 15 convex point bars and 2 concave counter point bars, relative to downstream (Fig. 7D). Individual abandoned channel (oxbow lake) fills surround 8 of the bars and are highly sinuous in nature. The point bar and counter point bar deposits range from 3.5 to 10 km long and 2 to 7 km wide, and the abandoned channel fills range from 400 to >1000 m in width, with an average width of 600 m. The meander-belt deposit thickness ranges from 35 to 50 m, and abandoned channel fills are 5 to 35 m thick (Fig. 7B).

METHODS

The migration of a series of meander bends on the Ucayali River, Peru, was captured in successive satellite images over a span of 24 yr (Fig. 3). The direct observation of river migration over time defines the basis for our analysis of all meander belts studied. This example shows that the net migrated area between successive channel locations, and areas of erosion due to continued migration, can be quantified (e.g., Figs. 3D and 3F). The Peruvian example provides a proof of concept that we will apply to the data sets in this study going forward. Application of this concept to each data set is explained in detail in Figure 8.

Paleochannel Reconstruction

We approached the data sets in order of increasing uncertainty so information from each successive study could be applied to enhance interpretations of less-informed data sets. Meander-belt topography and internal point bar architecture are critical to the reconstruction of channel paths and were utilized, where possible, in all data sets (Fig. 8). First, we considered the numerical model of van de Lageweg et al. (2016) as seen in Figure 5. Using planform topography maps generated for 50 yr time increments, we analyzed migrated channel paths to characterize bar accretion and erosion over ~750 yr of meander-belt evolution (Fig. 8A). The numerical model data set is advantageous in that there is little interpretation required to determine paleochannel locations for each stage. The limitations of this data set are inherent to the model parameters and the degree to which the model represents real-world meandering river processes, and the limited time span over which the model was run.

In our analysis of modern and recent deposits of the Mississippi River at New Madrid, Missouri (Fig. 6B), we used RC and OSL dates (Table 1), floodplain topography, and crosscutting relationships to map paleochannel locations over the last ~8000 yr (Fig. 8B). Sample ages and locations were used in conjunction with a range of known migration rates in order to interpret channel locations (Fig. 8B). A paleochannel location was reconstructed every 500 yr from the modern Mississippi River to 8000 yr B.P. The analysis of age-constrained scroll bar and abandoned channel deposits from New Madrid, Missouri, informed the reconstructions based on less-informed data sets (e.g., Helena, Arkansas, and McMurray Formation, Canada).

Further downstream in the Mississippi River Valley (Fig. 6E), we employed the methods and results of Fisk (1944) to reconstruct channel migration patterns at Helena, Arkansas. The maps produced by Fisk (1944) are the basis for reconstruction of 16 stages of Mississippi River migration (Fig. 8C). For each stage, discontinuously preserved deposits mapped for each paleochannel were identified, and a sinuous channel was fitted through these deposits in order to interpret a complete paleochannel outline (Fig. 8C). Adjacent paleochannel positions, scroll patterns, and aerial photographs were used to augment interpretations (Fig. 6D). The Fisk (1944) data set lacks age control beyond relative dating through crosscutting relationships. However, in consideration of the New Madrid, Missouri age control, the clarity of the scroll patterns in the satellite imagery, and detailed field mapping conducted by Fisk (1944) allowed for detailed channel locations to be interpreted with confidence. Comparison of the New Madrid, Missouri, dates to the reconstruction of Fisk (1944) suggests that Fisk's proposed 100 yr time interval between reconstructed stages was perhaps underestimated. Based on the oldest material at New Madrid, Missouri, and maps from Saucier (1994), we assume the deposits at Helena, Arkansas, are of a similar age range (8000 yr B.P. to present).

The two study areas from the Mississippi River meander belt were selected due to similarity in planform expression of a complex amalgam of point bars and abandoned channels to those apparent in seismically imaged strata of the Cretaceous McMurray Formation (Fig. 7C).

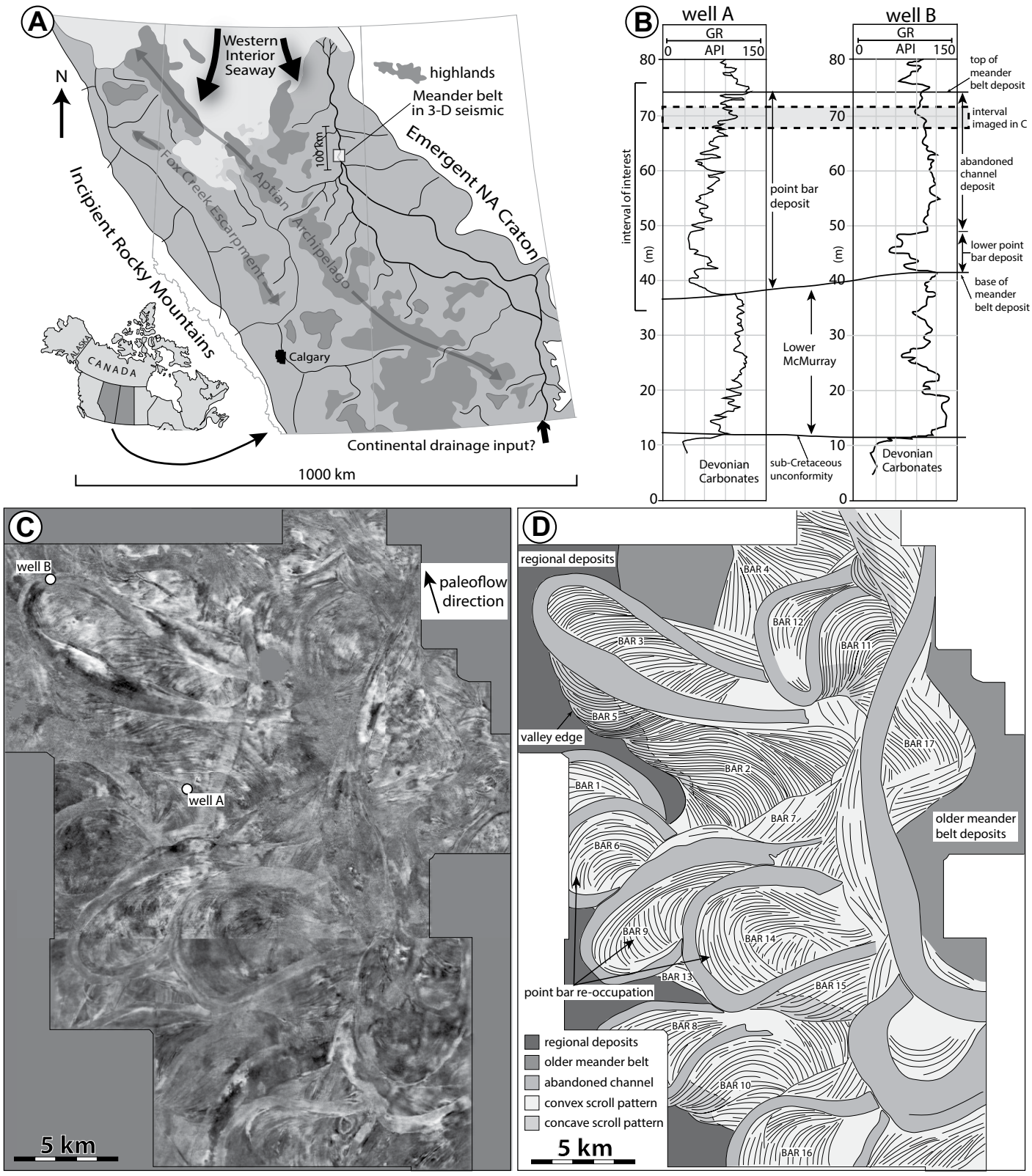

Figure 7. McMurray Formation data set (Lat: 56°6′32.94″N, Long: 110°55′17.33″W). (A) Location and paleogeography of the Alberta Basin during the Early Cretaceous. NA—North American. (B) Gamma-ray (GR) log signatures from well A and well B shown in C. (C) Three-dimensional (3-D) seismic stratal slice of the upper portion of the McMurray Formation characterized by point bar, counter point bar, and abandoned channel deposits. The interval imaged seismically in C is denoted by the gray dashed box in B. (D) Line tracing of the scroll patterns and abandoned channels present within the seismic stratal slice. Numbering of the bars refers to Table SD1 (see text footnote 1).

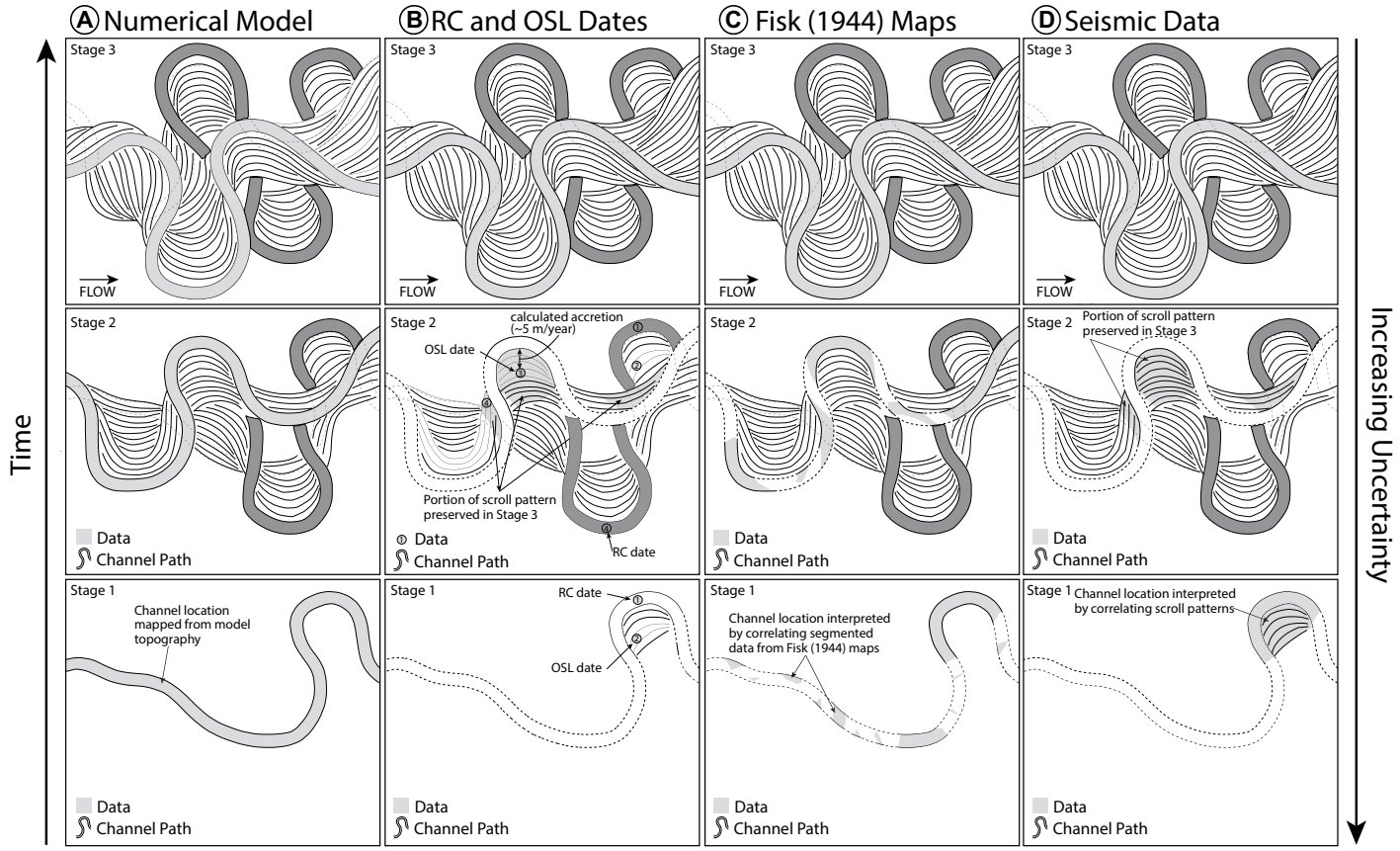

Figure 8. Comparison of methods used to reconstruct migrating channel locations. A qualitative example meander belt is used for simplicity and is the same for all data sets. (A) Numerical model—channel location mapped directly from topography maps generated at each time step. (B) New Madrid, Missouri—channel location interpreted based on radiocarbon (RC) and optically stimulated luminescence (OSL) dates from abandoned channel and scroll bar deposits, respectively. A net migration rate of ~5 m/yr was used to constrain channel locations (Holbrook et al., 2006). Scroll bar topography was also used to guide channel interpretations. (C) Helena, Arkansas—channel locations interpreted from segmented data from the maps of Fisk (1944). (D) McMurray Formation—channel locations interpreted from scroll patterns evident in seismic stratal slices. Crosscutting relationships indicate the relative age of bars, and bars with matching scroll patterns are correlated (e.g. Durkin et al., 2017).

Methods of seismic interpretation were consistent with other studies of fluvial deposits captured in 3-D seismic surveys (e.g., Hart, 2013). Initial morphologic characterization of McMurray Formation 3-D seismic stratal slices revealed relative ages of meander-belt elements through crosscutting relationships (Fig. 7D; Durkin et al., 2017). Like that of Fisk (1944), the subsurface data set also lacks specific age information for meander-belt elements. Following Fisk's workflow, 12 successive stages of evolution were interpreted for the McMurray Formation (Figs. 7D and 8D). As a result of the current inability to date the Cretaceous strata at millennial-scale resolution, the intervals separating the identified stages were qualitatively chosen in order to match spatial migration magnitudes of the stages from the age-constrained lower Mississippi River, New Madrid, Missouri, data set (Fig. 6C). This assumption is supported by interpretations of meander-bend migration of 30–65 m/yr for the McMurray Formation meander belt reported by Musial et al. (2012), who also made the comparison to observed rates on the lower Mississippi River (e.g., Hudson and Kesel, 2000).

Durkin et al. (2017) recently demonstrated that the high-quality nature of the 3-D seismic data, specifically, the readily visible lateral accretion patterns and abandoned channel margins, allows for detailed bar morphology to be reconstructed with confidence. Relative bar migration directions were validated by image data from wireline logs, which characterize bedding dip azimuth and angle (Muwais and Smith, 1990; Fustic, 2012; Brekke et al., 2017; Durkin et al., 2017). Key additional information included position of mudstone-filled abandoned channel fills and adjacent bar accretion patterns. The reconstructed channel planforms were typically highly constrained by the aforementioned data; however, in some instances, alternative interpretations are plausible. The highest uncertainty lies in the correlation between bars that are not adjacent nor linked by accretion patterns. The margin of error for channel correlations between bars is likely within 1–2 accretion surfaces (50–150 m) and would not significantly impact the quantitative results (Fig. 8D).

Preservation Calculations

From the numerical model (NAYS2D), the Mississippi River at Helena, Arkansas, and the Cretaceous McMurray Formation, a series of quantitative metrics derived from successive reconstructed paleochannels were considered, including: the net area of migration (MA), area preserved (PA), and the percent area preserved (PA/MA). Quantitative metrics for preservation

were not calculated for New Madrid, Missouri, due to the high degree of reworking and lack of evident scroll patterns in satellite images. Migrated area (MA) was measured from the inner bank of stage X-1 to the inner bank of successive stage X (Fig. 9A). Preserved area is a measurement of the original migrated area that has not been subsequently eroded by continued channel migration (Fig. 9A). Final preserved area was calculated at the final stage for each data set (Fig. 9). This approach was done on the accretion-package scale, the bar scale, and the meander-belt scale for all three data sets (Fig. 4). The definition of the meander-belt scale employed in this study is not consistent with all other published examples; however, it is similar to that of Blum et al., (2013). In this study, our meander-belt measurement represents the total net migrated area on all meander bends for each stage plus the preserved area of all previous stages (Fig. 4). Therefore, the number of measurements is equal to the number of evolutionary stages reconstructed.

We recognize that preservation is ultimately a three-dimensional problem; however, at the scales of investigation presented here, we are confident that the two-dimensional (2-D) planform analysis is an effective metric for preservation and provides a basis for comparison between data sets. A three-dimensional analysis is not feasible with the data available for all of the study areas, and vertical aggradation is minimal to nonexistent in the single-story meander-belt examples presented herein (cf. Blum et al., 2013; Jobe et al., 2016); therefore, area is a suitable surrogate for volume in this application.

In this analysis, the channel locations between reconstructed stages are not completely accounted for, and this is a source of measurement error. In Figure 9A, for example, during the time period over which accretion package F was deposited, both erosion and deposition occurred around the meander bend. Through the gradual migration of the meander bend during the time period over which channel 2 and channel 3 were active, some of the migrated area is eroded before the channel reaches position 3, and this is not accounted for in the net migrated

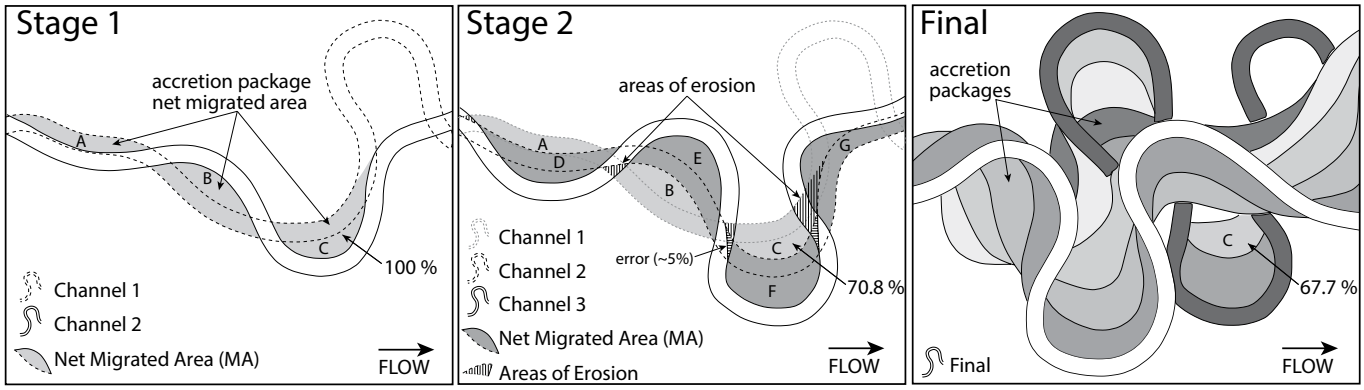

B

Stage	Stage (normalized)	Accretion Package	Migrated Area (m^2)	Preserved Area (m^2)	Preservation Percent
1	1	A	40 872.9	40 872.9	100.0 %
2	2	A		39 035.1	95.5%
⇣	⇣				⇣
Final	Final	A		0.0	0.0 %
1	1	B	76 935.0	76 935.0	100.0 %
2	2	B		72 726.5	94.5 %
⇣	⇣				⇣
Final	Final	B		0.0	0.0 %
1	1	C	75 245.4	75 245.4	100.0 %
2	2	C		53 259.2	70.8 %
⇣	⇣				⇣
Final	Final	C		50 955.4	67.7 %
2	1	D	70 678.4	70 678.4	100.0 %
⇣	⇣				⇣
Final	Final	D		0.0	0.0 %

Figure 9. Methods used for calculating migrated area (MA), preserved area (PA), and percent preservation. (A) Stage 1 documents the net migrated area of accretion packages A, B, and C. Stage 2 documents the migration of D, E, and F, and the erosion of accretion packages A, B, and C due to natural migration of the meandering channel. Stages between stage 2 and final are not shown. The final stage documents the preservation of accretion packages A, B, and C, where A and B have been completely eroded (preservation of 0.0%) and C is 67.7% of its original migrated area. (B) Table of metrics calculated for accretion packages from part A, including net migrated area, preserved area, and preservation percent. All measurements and calculations for each study area are included in the supplementary data tables (see text footnote 1).

area measurement of accretion package F. The magnitude of this error calculated from a series of accretion packages was <5% of the total migrated area, and it was consistent among the various bars analyzed in each of the data sets. We used "net migrated area" to describe the metric calculated.

RESULTS AND ANALYSIS

Numerical Model—NAYS2D

Sixteen successive stages of channel migration and evolution were mapped directly from topographic surface model outputs (Fig. 8A). Each stage represents the channel location at that time, and each successive stage documents ~50 yr of meander migration. Each stage is characterized by a sinuosity value and a series of active bars, where stage 1 (t = 293) is the oldest, and stage 16 (t = 668) is the final stage (Table 2; Fig. 10). The area of bar growth and subsequent area of preservation were documented. Important evolution events include the following: (1) Initial stages of channel evolution are dominated by low sinuosity (Table 2) and lateral bar migration. (2) Meander loop cutoff of bar 2 results in rotation of the accretion direction in bar 1 and initiates downstream translation (Fig. 10B). (3) At stage 568, two meander loops are cut off, which causes morphologic changes in bars upstream and downstream of the cutoffs (Fig. 10). (4) The final three stages are characterized by modest migration among the upstream bars, compared to earlier stages of evolution.

In total, 133 accretion packages (APs) from 21 individual bars were analyzed (Fig. 10B). All of the bars were active for two or more stages of evolution, while bar 1 provided the most continuous data over stages 1–13 (Table SD1[1]). For all APs analyzed, the MA values ranged from 0.01 km^2 to 0.23 km^2, and the final percent preservation values ranged from 0% to 100% (Table SD1 [see footnote 1]). The average preservation percent (PA) of an AP was 65.8% with a standard deviation of 31.8%.

The final percent preservation values did not follow a consistent trend throughout the evolution of the meander belt. Many of the bars exhibited an increasing preservation percentage over time (e.g., bars 14, 15, 16, 20; Table SD1 [see footnote 1]); however, other bars were not characterized by such a trend (e.g., bars 1, 4, 7; Table SD1 [see footnote 1]). A limitation with this data set is the short time span over which the simulation was run; only four bars reached the point of abandonment (bars 2, 9, 15, 19; Fig. 10B), and very little subsequent erosion took place. However, a benefit of this data set was the difference in MA versus PA, which was almost entirely due to intra-meander-bend erosion (Fig. 9A; e.g., Durkin et al., 2015), i.e., not due to subsequent erosion by a new meander loop cannibalizing an older one. This provides insight into the proportion of erosion that occurs within a meander loop, compared to subsequent erosion of APs once the meander loop has been abandoned, which will be discussed later.

TABLE 2. SINUOSITY VALUES FOR EACH STAGE OF CHANNEL RECONSTRUCTION FROM ALL THREE DATA SETS

Study area	Stage	Valley length (m)	Channel length (m)	Sinuosity
NAYS2D	1	3510.26	5270.6	1.5
NAYS2D	2	3340.57	6014.67	1.8
NAYS2D	3	3251.96	6446.18	1.98
NAYS2D	4	6039.3	8171.5	1.35
NAYS2D	5	6796.43	10,350.2	1.52
NAYS2D	6	7922	11,815.6	1.49
NAYS2D	7	7945	13,256	1.67
NAYS2D	8	8392.41	15,125.2	1.8
NAYS2D	9	7831.81	16,112.3	2.06
NAYS2D	10	7998.38	18,353.4	2.29
NAYS2D	11	9111.04	17,622.1	1.93
NAYS2D	12	9118.56	15,482.3	1.7
NAYS2D	13	9070.7	17,820.3	1.96
NAYS2D	14	9132.21	19,796.7	2.17
NAYS2D	15	9073.38	20,784.6	2.29
NAYS2D	16	9034.26	21,743.7	2.41
Helena, AR.	4	23,174	60,694	2.62
Helena, AR.	5	25,287	39,750	1.57
Helena, AR.	6	25,187	50,418	2
Helena, AR.	7	24,856	48,195	1.94
Helena, AR.	8	22,006	58,038	2.64
Helena, AR.	9	22,241	63,538	2.86
Helena, AR.	10	24,134	59,028	2.45
Helena, AR.	11	26,510	74,551	2.81
Helena, AR.	12	23,673	78,286	3.31
Helena, AR.	13	24,356	56,915	2.34
Helena, AR.	14	24,120	50,424	2.09
Helena, AR.	15	24,137	45,212	1.87
Helena, AR.	16	20,642	48,244	2.34
Helena, AR.	17	23,727	54,896	2.31
McMurray Fm.	1	30,309	51,028	1.68
McMurray Fm.	2	30,151	67,188	2.23
McMurray Fm.	3	30,178	76,590	2.54
McMurray Fm.	4	31,688	77,128	2.43
McMurray Fm.	5	32,128	80,930	2.52
McMurray Fm.	6	32,005	62,206	1.94
McMurray Fm.	7	30,737	59,387	1.93
McMurray Fm.	8	30,758	62,983	2.05
McMurray Fm.	9	30,087	77,585	2.58
McMurray Fm.	10	28,899	75,495	2.61
McMurray Fm.	11	25,561	36,744	1.44
McMurray Fm.	12	22,644	25,041	1.11

Note: AR.—Arkansas; McMurray Fm.—McMurray Formation, Alberta, Canada.

New Madrid, Missouri

Sixteen successive stages of evolution were reconstructed using OSL and RC dates, satellite images, and maps from Holbrook et al. (2006; see also Fig. 8B herein). OSL and RC dates provided high-quality constraints on deposit ages, which allowed for paleochannels to be mapped every ~500 yr B.P. (Figs 11A and 11B). The oldest dated material was 7499 (± 376) yr B.P. (Table 1); therefore, the oldest channel reconstructed was chosen to be 8000 yr B.P. All of the RC and OSL dates used are provided in Table 1. Important evolution events included the following: (1) the abandonment of the Portageville loop after 6500 yr B.P. (Figs. 6C and 11B); (2) the significant avulsion to the east that occurred after 4000 yr B.P. and lasted ~1500 yr before returning to its original course to the west (Fig. 11B); and (3) movement along the Reelfoot fault scarp that impacted channel sinuosity, causing a change from low to high sinuosity during times of fault slip and quiescence, respectively (Table 1; Holbrook et al., 2006). This occurred concurrent with decreases in sinuosity after ca. 4250 yr B.P. and ca. 1900 yr B.P. (Figs. 6C and 11B). A high degree of channel reworking and lack of scroll pattern detail from satellite images due to intense agricultural activ-

[1]GSA Data Repository item 2017379, all measurements of migrated area, preserved area and preservation percent, as well as the data used to construct graphs in Figure 14. An additional figure to explain how graphs in Fig. 14 were constructed is also included; Table DR1, DR2, Figure DR1, is available at http://www.geosociety.org/datarepository/2017 or by request to editing@geosociety.org.

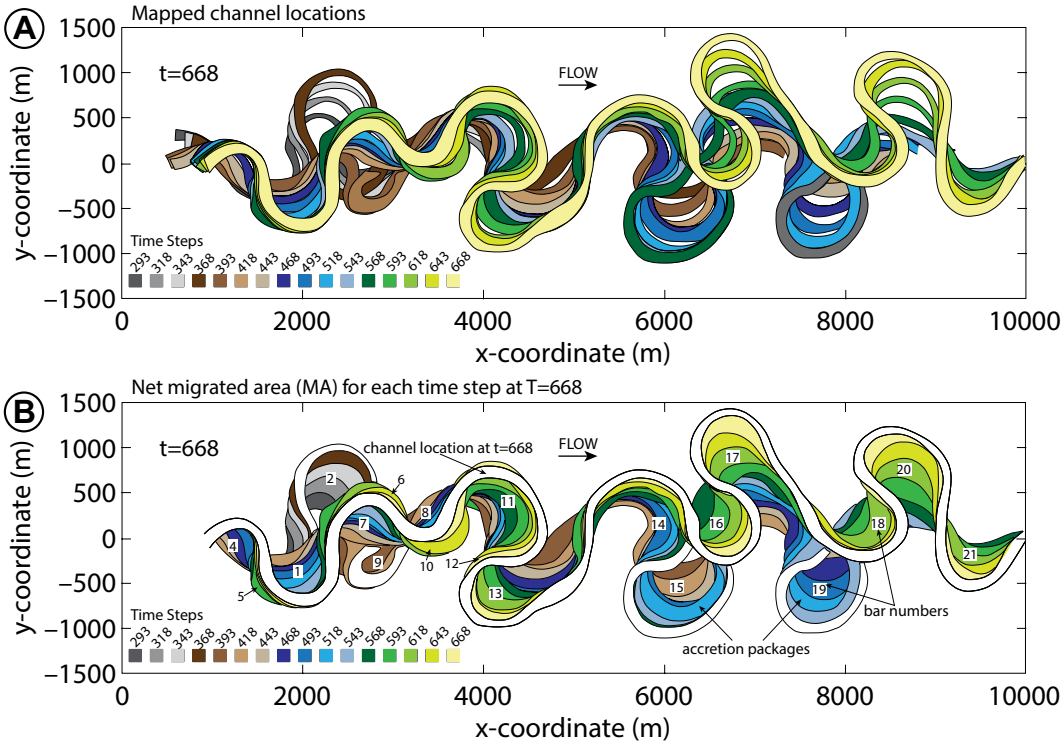

Figure 10. Results from the numerical model channel mapping. (A) Mapped channel locations for each stage from *t* = 293 to *t* = 668. (B) Interpretation of the accretion packages preserved over the evolution of the model from *t* = 293 to *t* = 668. Bar numbers are indicated.

ity made it difficult to interpret bar morphology and paleochannel geometries. Therefore, quantitative metrics of preservation were not calculated for this data set. The high-precision age control from New Madrid, Missouri, is important, however, because it informs the time span of the other data sets.

Helena, Arkansas

Sixteen successive stages of evolution were reconstructed to account for the deposits preserved on the meander plain north of Helena, Arkansas (Fig. 8C). Each stage was characterized by a sinuosity value and a series of active bars, where Fisk's (1944) stage 4 represents the oldest, and the modern Mississippi represents the youngest channel location (Table 2; Fig. 11D). Stages prior to stage 4 were not able to be reconstructed with confidence due to lack of preservation and were therefore not analyzed. A sinuosity measurement for each stage (Table 2) and metrics for migration from stage X-1 to stage X were calculated (Table SD1 [see footnote 1]). Important evolution events included the following: (1) Initial stages of evolution were characterized by lateral migration and expansion of active bars, generally migrating away from the center of the meander belt (Fig. 11D). (2) The sinuosity values did not follow a significant trend and remained relatively consistent, between 1.57 (stage 5) and 2.86 (stage 9), with one outlier of 3.31 at stage 12 (Table 2; Fig. 11D). (3) Two successive meander-loop neck cutoff events occurred during two successive stages of evolution. Bar 5 was cut off at stage 13, and the immediate downstream bar 6 was cut off at stage 14 (Fig. 11D). (4) Stages 5, 6, and 7 document the lateral migration and expansion of a meander loop in the south-central portion of the study area. This loop was cut off after stage 7; however, stages 8 and 9 reoccupied the same meander loop location and deposit bar 7 (Fig. 11D). (5) The final stages (stages 14–19) were dominated by downstream migration, which is evident in the scroll bar patterns of bars 17, 18, and 19 (Fig. 11D).

All of the 19 bars documented were active for two or more stages of evolution, and 54 APs were measured. Bars 5 and 6 provided the most continuous data over stages 6–11 and 7–12, respectively (Table SD1 [see footnote 1]). For all bars analyzed, the MA values ranged from 1.0 km^2 to 48.4 km^2, the PA values ranges from 0.0 to 10.0 km^2, and the final percent preservation values ranged from 0% to 100% (Table SD1 [see footnote 1]). The average final preservation percent of an AP was 27.3% with a standard deviation of 34.1%.

The MA values were not characterized by a notable trend through the entire evolution of the meander belt and were commonly within one order of magnitude between successive stages for an individual bar. In some instances, migrated area decreased significantly between successive stages, for example, in bars 2 and 4 (Table SD1 [see footnote 1]). In both examples, the decrease in MA occurred in the final stage of migration, which may be explained by partial cutoff and decreased energy, minimizing outer bank erosion and point bar accretion (cf. Toonen et al., 2012).

The preserved percent values for individual bars were characterized by an increase in preservation percent as the bar migrated for most of the bars studied. In some instances, none of the interpreted bar was preserved (bar 3), and often very little to no evidence of the initial stages of growth was preserved (bars 2, 5, 6, 12, 17; Fig. 11C; Table SD1 [see footnote 1]). This was likely controlled by the length of time each AP was subjected to potential erosion, where older portions of the point bar were reworked by subsequent channel migration of the same meander loop. Another possible contributing factor is a typical bar will laterally migrate away from the meander belt axis, and reoccupation probability decreases away from the center of the meander belt (van de Lageweg et al., 2016). This is a common theme between individual bars as well, where bars are more likely to be preserved away from the middle of the meander belt, for example, bar 3 versus bar 5 (Fig. 11C).

Early Cretaceous McMurray Formation

Twelve successive stages of evolution were reconstructed to account for the deposits preserved in the (subsurface) McMurray Formation (Figs. 7 and 8D). Each stage represents a

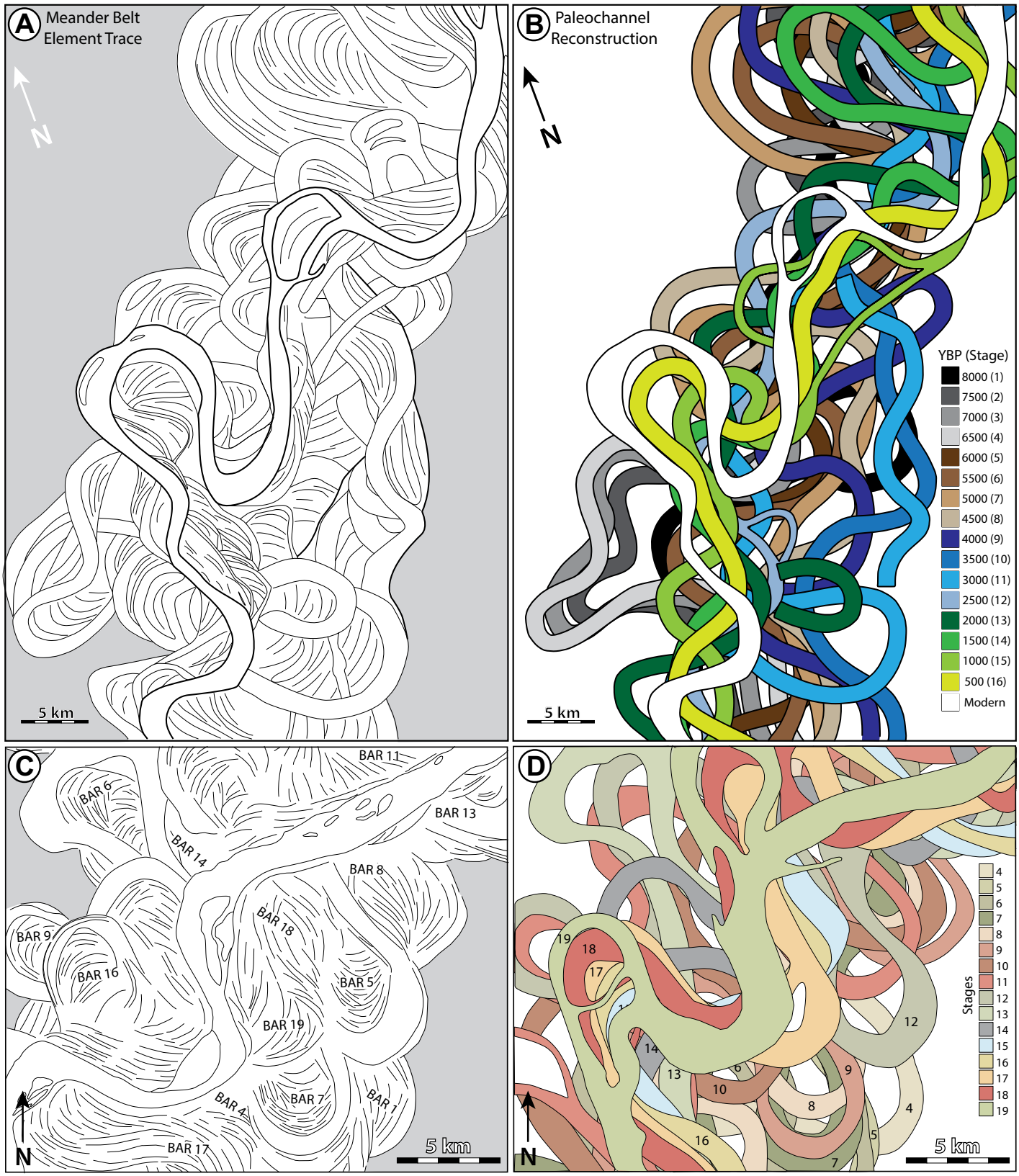

Figure 11. Mississippi River meander-belt study area results. (A) New Madrid, Missouri, meander-belt element trace using data from Holbrook et al. (2006) and satellite imagery. (B) Reconstructed paleochannels every 500 yr from present day to 8000 yr B.P. (C) Helena, Arkansas, meander-belt element trace from satellite images and Fisk (1944). (D) Nineteen stages of reconstructed paleochannels (modified from Fisk, 1944). YBP—yr B.P.

channel location, where stage 1 is the oldest, and stage 12 is the youngest. Stages were characterized by a sinuosity value and a series of active bars (Fig. 12; Table SD1 [see footnote 1]). The migration of active bars from stage X-1 to stage X and associated changes in sinuosity are represented in Table 2. Important evolution events included the following: (1) increasing sinuosity from 1.68 at stage 1 to 2.52 at stage 5, which resulted from continued lateral migration of active bars 2, 3, and 4 (Table 2; Fig. 12); (2) development of a counter point bar downstream of bar 2 from stage 2 to stage 3, which was coincident with the cutoff of bar 1 (Fig. 12); (3) neck cutoff of bar 3 at stage 6, resulting in a significant decrease in sinuosity from 2.52 at stage 5 to 1.94 at stage 6 (Table 2; Fig. 12); (4) some degree of reoccupation of previous bar locations for bars 1, 5, 10, and 11, in an overall easterly direction (Fig. 12); and (5) a continued overall decrease in sinuosity from 2.61 at stage 10 to 1.11 at stage 12, caused by meander cutoffs and a relative dominance of downstream migration in active bars (Table 2; Fig. 12). The final channel position (stage 12) had a very low sinuosity (1.11).

All of the 17 distinct bars were active for two or more stages of meander-belt evolution, and 60 APs were measured (Table SD1 [see footnote 1]). Bar 7 provided the most continuous data over stages 5–10. For all bars investigated, the MA values ranged from 0.3 km^2 to 20.4 km^2, the PA values ranged from 0.0 to 13.4 km^2, and percent preservation values ranged from 0% to 100% (Table SD1 [see footnote 1]). The average final preservation percent of an AP was 52.8% with a standard deviation of 35.1%.

Values of MA between stages for individual bars were often within an order of magnitude and did not follow any notable trends throughout meander-belt evolution (Table SD1 [see footnote 1]). Percent preservation values were characterized by a common trend expressed at two different scales. On individual bars, successive stages showed an increase in percent preservation as the meanders grew. This was due to the common erosion of early products of bar growth due to downstream erosion, and increases in meander-bend sinuosity. A similar trend was noticed at the meander-belt scale, where younger bars yielded higher preservation percentages than relatively older bars. This is an intuitive result, because older bars have more time to experience erosion and reworking than younger bars. Although difficult to document due to the lack of eastern valley edge constraint, it also appears that the distance from the middle of the meander belt may also have played a key role in preservation potential, as bars deposited away from the center of the meander belt were also less reworked (cf. van de Lageweg et al., 2016).

Common Themes Among Data Sets

Through comparison of meander-belt evolution from each of the data sets, common themes are evident. As discussed, all of the data sets were characterized by increasing preservation

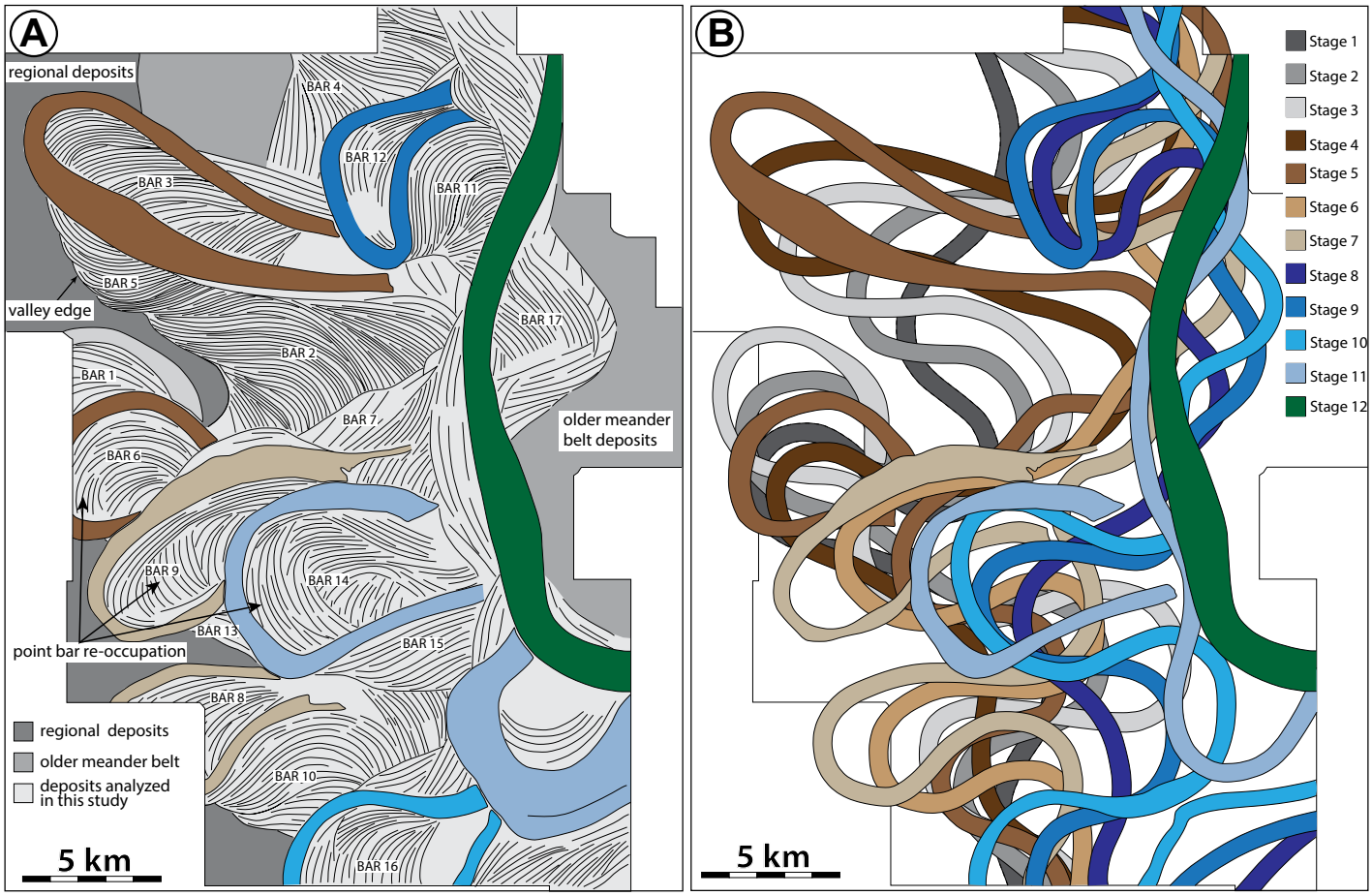

Figure 12. Stages of evolution for the McMurray Formation meander-belt deposits. (A) Line trace of meander-belt elements from seismic stratal slice in Figure 7C. Color of abandoned channel-fill deposits refers to associated stages of evolution from part B. (B) Twelve stages of reconstructed paleochannel locations interpreted from accretion patterns, crosscutting relationships, and positions of abandoned channel deposits evident in three-dimensional seismic data (Fig. 7C; Durkin et al., 2017).

percent for APs from oldest to youngest within an individual bar and between bars as meander belts evolved. This is explained by the length of time each AP was subjected to potential erosion by subsequent channel migration, where older APs and bars would be more likely to be eroded than younger ones.

The paleochannel evolution analysis highlights the reoccupation of recently abandoned point bar deposits in the Helena, Arkansas, and McMurray Formation data sets. Several examples from these data sets were characterized by the development of a point bar over several stages, which was then cutoff through normal neck or chute cutoff processes (e.g., Figs. 11C, 11D, and 12). However, in the following stages, a new point bar grew in the same direction and location as the previous, recently abandoned point bar (Fig. 12). This process was likely controlled by the relatively uncompacted sediment of the previous point bar, which allowed for easy erosion of the cutbank and reworking of the previous point bar material (Perruca et al., 2007). Another controlling factor may have been that the abandoned meander loop was not completely filled with sediment and would have provided less resistance to erosion compared to completely filled erosion-resistant fine-grained abandoned channels elsewhere in the meander belt. The result was often several nested, successive point bar and abandoned channel deposits (e.g., McMurray bars 1, 6, 9, 14; Fig. 12A).

A comparison of preservation among all of the data sets yielded a series of key observations (Fig. 13). For the numerical model (NAYS2D), many of the AP preservation percentages were above 70%, and the 100% bin contained three times more than any other bin (Fig. 13). For the Helena, Arkansas, data set, the highest frequency bin was 0.0% preservation, and the data were slightly more frequent for values of <35%, except for the 100% bin (Fig. 13). The McMurray Formation data set did not exhibit any recognizable trends; however, the highest frequency bin was 100% (Fig. 13). The similarity in distributions and values between the Mississippi River and McMurray Formation meander belts helps to strengthen the analog interpretation. The numerical model analysis yielded specific results because of the limited duration of the NAYS2D model meander belt (~750 yr of meander migration); the Mississippi River at Helena, Arkansas, data set documents ~8000 yr. We do not have age control on the McMurray Formation meander belt; however, due to the similarity in size and scale, we estimate the time span to be on the same scale as the Mississippi River segments studied.

The numerical model data document the magnitude of erosion due mainly to intra-meander-loop processes (e.g., Brice, 1974; Diaz-Molina, 1993; Nardin et al., 2013; Durkin et al., 2015), since the time span of the data is insufficiently long to document inter-meander-loop processes. This would suggest that the magnitude of erosion due to intra-meander-loop processes may be significantly less than inter-meander-loop processes. In well-developed meander belts, these processes would be ongoing simultaneously, since meander loops are constantly being cut off and subjected to inter-meander-loop erosion, while continued channel migration would result in intra-meander-loop erosion. The numerical model example is specific in that the initial stages of channel migration begin from a straight channel, and thus channel migration is not eroding previous meander-belt deposits. It is not until meander loops reach the point of cutoff that we observe inter-meander-loop processes. This would not be the case in other examples studied, since the window of observation occurs after initial stages of channel meandering.

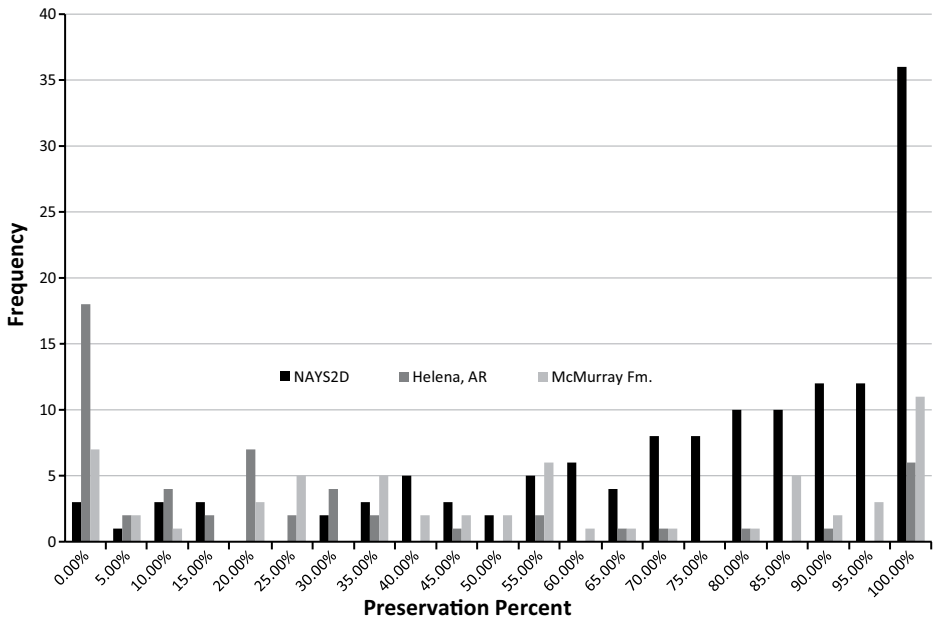

Figure 13. Histogram of the preservation percent of accretion packages for all three data sets. AR—Arkansas.

DISCUSSION

Paleochannel reconstructions provide insight into the evolution of fluvial meander-belt deposits (Durkin et al., 2017). However, detailed paleochannel reconstructions have not been previously attempted for deep-time deposits at the meander-belt scale, in part due to the lack of obvious data with which to constrain successive channel locations. The examples documented here provide a methodology for attempting reconstructions from a wide range of data types at various temporal and spatial scales. We present this analysis as a novel tool for any stratigraphic characterization in order to test the validity of an interpretation. For example, if the interpretation of a fluvial system from the available data cannot be reproduced though the evolution of a migrating and continuous channel thread, then the stratigraphic interpretation should be reconsidered.

Reconstruction of the time-step evolution for a sedimentary sequence is also applicable to sedimentary systems outside of meandering fluvial deposits, such as a progradational shoreline profile (e.g., Wheeler, 1958). Mahon et al. (2015) investigated the stratigraphic completeness of delta shoreline trajectories on a 2-D dip-parallel cross section of an experimental delta; their study was a cross-sectional example analogous to the planform method described here. Any 3-D data set where crosscutting relationships are evident provides a basis for an evolutionary reconstruction and has the potential to vastly improve stratigraphic interpretations, paleoenvironment reconstructions, and understanding of preservation potential.

"Survivability" of a Sedimentary Body

The topic of stratigraphic completeness has received significant recent attention (Straub and Esposito, 2013; Miall, 2014a; Sadler and Jerolmack, 2014; Smith et al., 2015; Mahon et al., 2015). Many studies have noted the inherent difficulty in understanding linkages between modern observations of sedimentary systems and the product in the rock record. The difficulty lies in

the gaps in the rock record, where researchers often have little indication of the magnitude and duration of the gaps (Fig. 1). Many processes that result in gaps in the rock record occur at time intervals longer than human observation, and therefore they are relatively poorly understood (Schumer and Jerolmack, 2009; Miall, 2014a). This is true for many aspects of the geologic record beyond fluvial sedimentology, such as the detailed measurements of climate change that can be documented by humans versus the level of detail revealed in ancient strata (Kemp et al., 2015). We hypothesize that quantification of the preservation of sedimentary bodies in a range of examples will improve our understanding of the processes governing preservation and ultimately stratigraphic completeness for a breadth of sedimentary systems.

The ratio of sediment deposited versus sediment preserved provides quantitative data for the "survivability" or decay rate, and a maximum preservation percent for accretion packages, individual bars, and meander belts (Table SD2 [see footnote 1]). These data inform the likelihood for erosion of these deposits, or their "survivability" (i.e., preservation potential; Fig. 14) over time. For the data considered, the independent variable is stage (normalized), which is representative of dimensionless time, and the dependent variable is preservation percent (Fig. 14). It is important to note that all deposits measured were normalized to begin at 100% preservation, where stage = 1. These graphs track the sedimentary bodies through time, where they can either remain at 100% or decrease to some final preservation percent of their original migrated area, which may be 0% (Fig. 9; Table SD2 [see footnote 1]).

The first, and perhaps most important observation, is that all of the graphs are characterized by the same general formula:

$$y = -(a)\ln(x) + 1. \quad (1)$$

The logarithmic decay of preservation percent is consistent regardless of spatial or temporal scale. The trend line was fit to the data with a y-intercept value stipulated as stage = 1 and preservation percent = 100% because all measurements start at that value. The fit of the trend line (correlation coefficient, r^2; Fig. 14) is weak at the accretion package scale (r^2 values of 0.22–0.31), due to the inherent variability of the system at this scale. As we increase the scale of investigation, the correlation coefficients improve to r^2 values of 0.78–0.82. Sadler and Strauss (1990) showed that the probability of preservation is also defined by $y = \ln x$ at the period scale (Fig. 2). Our data support the assertion that the average trends of completeness and preservation also follow a natural log function across all measured scales. This is a powerful conclusion that links real-world quantitative data to the theoretical models of Sadler and Strauss (1990), at these spatial and temporal scales. It is important to note that the graphical representation of the probability of preservation presented by Sadler and Strauss (1990) refers to a stratigraphic column, which includes the vertical dimension. Without a vertical component, preservation will tend to zero, as it does in the results of our study (Fig. 14), due to constant reworking of the meandering channel until the point of avulsion. Final preservation of a meander belt involves a component of vertical aggradation, which takes place at a longer time interval than those studied. Physically, aggradation is manifest as a series of two or more meander belts, and in our analysis, we only considered one in each example. As we increase the scale to several successive meander belts, we will need to incorporate factors such as avulsion rate, subsidence, relative sea-level fluctuations, aggradation rates, etc. (e.g., Straub et al., 2009). This type of information is not readily available from the data sets studied; therefore, we only considered here the dimensions and scales that we had sufficient ability to characterize.

Spatial and Temporal Scale Comparisons

The results summarized in Figure 14 allow for comparisons between data sets and across temporal and spatial scales. One important observation is the decrease in the spread of the data as the spatial scale increases from accretion packages (large spread) to meander belts (small spread) (Fig. 14). The systems show a trend toward more consistency of preservation for a specific stratal unit at higher hierarchical levels. This result is consistent with predictions by Miall (2014a), who suggested that as spatial and temporal scales increase, the randomness of autocyclic processes becomes less of a driver, and preservation becomes more dependent on allocyclic processes, which tend to be less random, and therefore the rates appear more normalized (Miall, 2014a; Sadler and Jerolmack, 2014).

The numerical model and Mississippi River data sets have relatively high-resolution temporal control (Holbrook et al., 2006; van de Lageweg et al., 2016), whereas the McMurray Formation data set has little to no temporal control. When comparing the preservation percent of the trend line at the last reconstructed stage of evolution, the numerical model preservation percent is consistently higher than the Helena, Arkansas, data set, at all spatial scales (Fig. 14). This is likely due to the fact that only the first portion of the overall average trend line for each spatial scale was captured (Fig. 15A), and in the short-time-span data set (i.e., numerical model – NAYS2D), the curve has not fully developed yet. However, if the general formula of $y = -(a)\ln(x) + b$ is consistent throughout the rock record, we can estimate the time span represented by the McMurray Formation deposits.

If we consider the accretion package scale for the Helena, Arkansas, data set, the curve reaches ~8% preservation at the last stage of evolution (Fig. 14B, stage 16). For the McMurray Formation data set, the curve reaches ~31% preservation (Fig. 14C, stage 12). If "survivability" functions are analogous for the McMurray Formation and Mississippi River depositional systems, the time span represented by the McMurray Formation would be approximately equal to the point at which the Helena, Arkansas, curve reaches ~31%, which is stage 8 (Fig. 14B). Therefore, if each stage is ~500 yr, the time span represented in the McMurray Formation is ~4000 yr. The assumption is that the time span represented by a meander belt can be determined by the degree of reworking of the deposits. It is important to note that for the McMurray Formation data set, only bars that were at least partially preserved were considered; presumably, bars from the early stages of evolution have been completely removed and thus could not be reconstructed. We predict that this would impact absolute values of preservation percent but not the shape of the "survivability" curve (Fig. 14), and thus the estimate of ~4000 yr would be a minimum age.

If we consider a generalized preservation curve for the rock record, the proportion of that curve captured by each of the data sets is hypothesized in Figure 15B. For all of the data sets, from accretion package, to bar, to meander-belt scales, we capture less of the representative survivability. This is due to the increasing length of time each successive spatial/temporal scale requires to fully develop a curve to the point where it either reaches zero or a constant percent preservation. Therefore, the results from the accretion package are perhaps the most representative of its true survivability curve, while the meander-belt scale requires a much longer window of observation to be characterized.

Preservation in the Rock Record

Fractal relationships are particularly common in geoscience, for example, earthquake magnitudes, fault and fracture lengths, the orders of sequence stratigraphy, etc. (Smith et al., 2015). In relation to completeness, Miall (2014a) summarized that sedimentation rates, stratigraphic gaps, and the distributions of layer thickness also have fractal-like properties (Plotnick, 1986; Sadler, 1999; Schlager, 2004; Bailey and Smith,

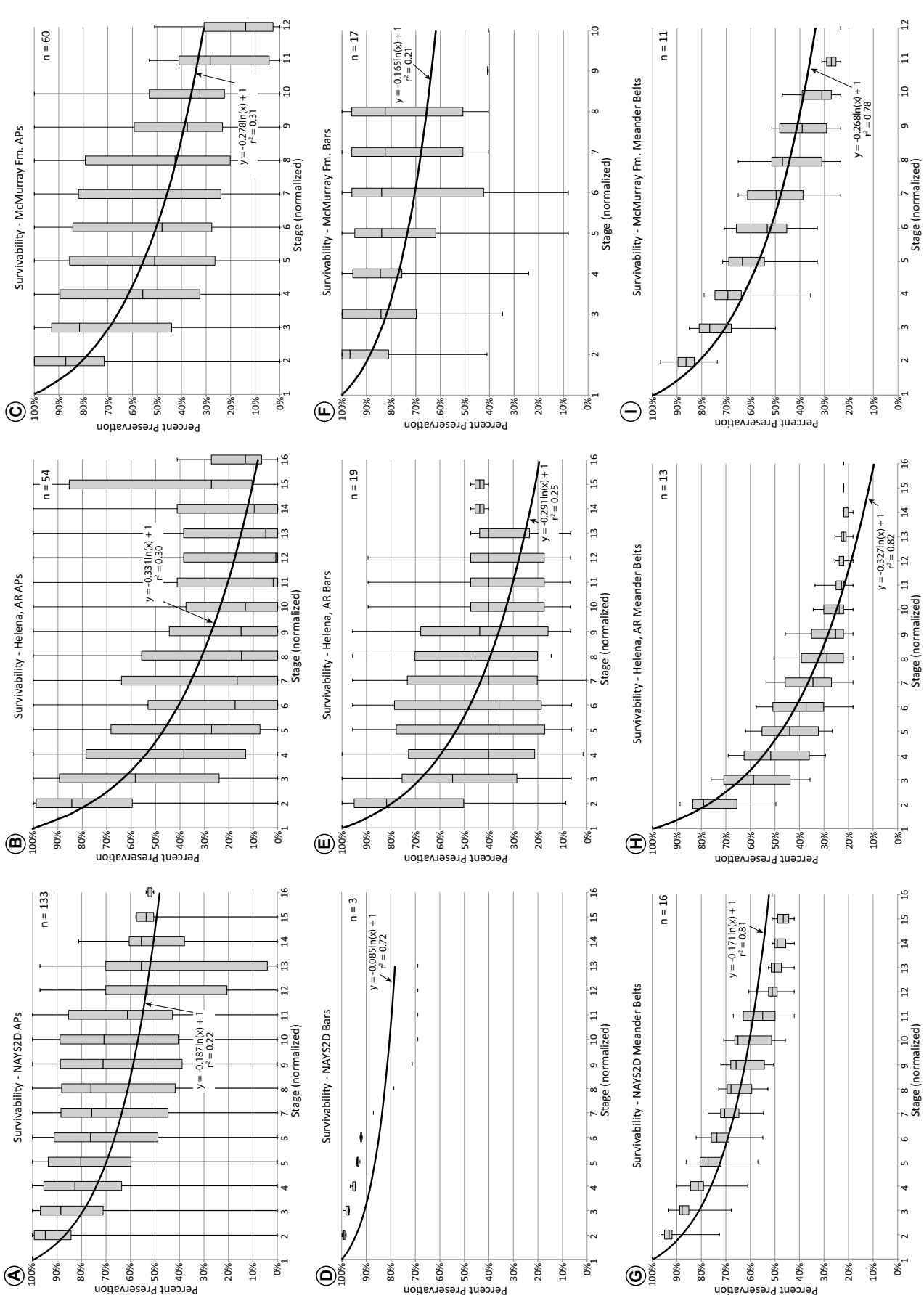

Figure 14. Series of "survivability" graphs showing percent preservation vs. time. Box-and-whisker plots represent results of preservation over time for individual accretion packages (APs) (A–C), bars (D–F), or meander belts (G–I). The thicker black line represents the trend line for each data set. Note that regardless of which stage APs, bars, or meander belts are deposited, all measurements are normalized to begin at stage = 1, and preservation percent = 100%. An example of the data for these graphs is presented in Figure 9. Raw data for the graphs can be found in Table SD2 (see text footnote 1). AR—Arkansas.

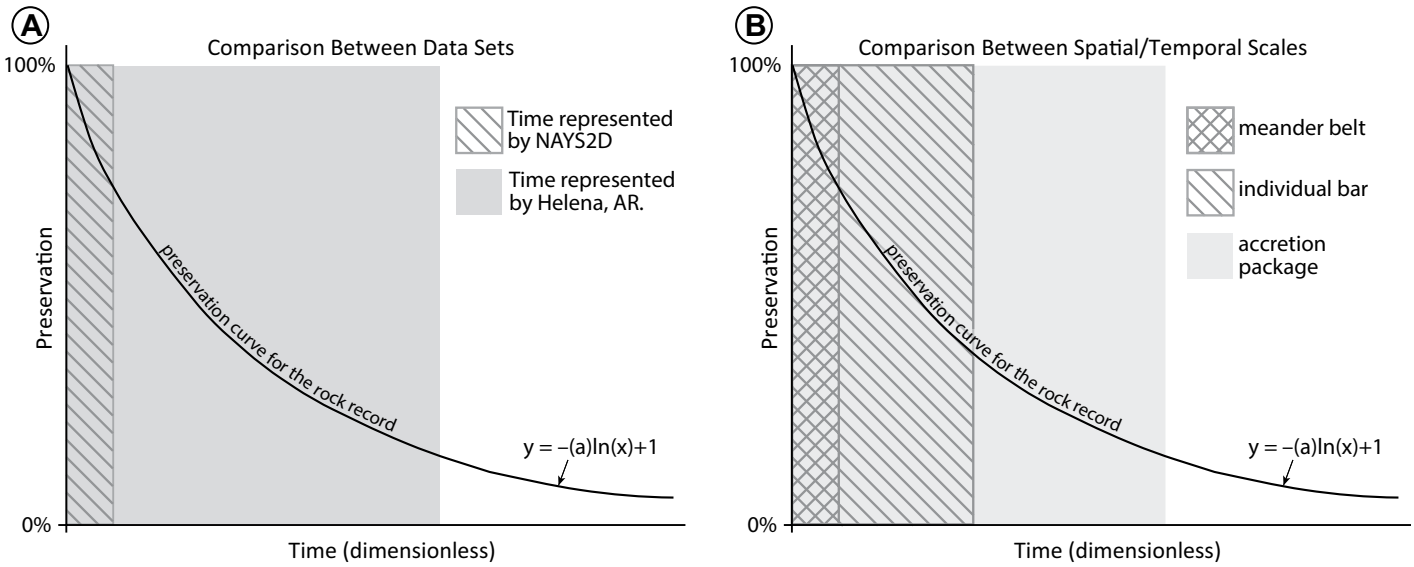

Figure 15. (A) Difference in time represented by the numerical model and Helena, Arkansas (AR), data sets. (B) Comparison of the relative proportion of the curve that is represented by each spatial and temporal scale.

2005, 2010: Miall, 2010). Sadler and Jerolmack (2014) also suggested that stratigraphic hiatuses are fractal, existing at all scales. This conclusion is based on a three-dimensional approach to understanding the constancy of global sediment flux rates by utilizing the effectively continual processes of denudation and deposition along entire sediment routing systems.

Our study of fluvial sediment routing system segments documents the rate of decay, or survivability, of a sedimentary body rather than the distribution of hiatuses. We found that at all scales measured, there is a self-similar, systematic, monotonic decrease in preservation with time. The probability of preservation over time was expressed as a natural log function by Sadler and Strauss (1990) for the entire rock record (Fig. 2). From the analysis presented here, when preservation curves are generated for a variety of scales and data sets, the data are also characterized by a natural log function. This may suggest that there is perhaps a fractal-like relationship for preservation in the rock record, where each scale of investigation informs the next larger spatial/temporal scale, and the natural logarithmic decay of preservation is characterized by self-similar geometry. However, in order to test this hypothesis, further studies at larger and smaller spatial scales, as well as longer and shorter temporal scales, are necessary.

CONCLUSIONS

We reconstructed the evolution of fluvial-meander belts using a variety of data sets and techniques to map successive stages of channel migration. The analysis reveals linkages between geomorphic processes and associated patterns of deposition and erosion. By reconstructing the paleochannel evolution of meander-belt deposits, we were able to quantify the proportion of sediment deposited versus that ultimately preserved in the rock record. This approach provides a new method for testing meander-belt interpretation viability by demonstrating the evolution with an actual evolving channel thread.

The completeness of the stratigraphic record is often considered in one dimension with average net accumulation rate as the dependent variable. We present a novel approach to the concept of stratigraphic completeness through 2-D planform analysis of fluvial-meander belts, measuring the preservation of a sedimentary body at three distinct spatial and temporal scales. By reconstructing the paleochannel evolution of meander-belt deposits, the subsequent erosion after deposition can be quantified until a sedimentary body reaches a final preservation percent (which may be zero); we have termed this "survivability." Characterization of the survivability curve reveals the processes responsible for decreasing the average sediment accumulation rates over time ("Sadler effect"). In the examples studied, these processes include intra-meander-bend erosion (due to downstream translation or bar rotation), increasing sinuosity and cutoffs (neck and chute), as well as inter-meander-bend erosion due to avulsion and subsequent migration of the meandering channel. The results of our analysis show that the average preservation percent of an accretion package ranges from 27.3% to 67.8%. Additionally, we estimated the time span represented by a meander-belt deposit based on the degree of reworking, derived from comparisons between survivability curves. This can be applied to deep-time strata, improving paleoenvironmental interpretations and our understanding of meander-belt processes over long time scales.

Our analysis captures the decrease in preservation of a fluvial sedimentary body over time, documented by the survivability curve. We find that the data are characterized by a natural logarithmic function of decay. The general formula $y = –(a)\ln(x) + b$ is consistent regardless of the spatial or temporal scale, which agrees with the probabilities of preservation at long time scales proposed by previous workers.

ACKNOWLEDGMENTS

Funding and seismic data for this project were provided by ConocoPhillips Canada, as well as a Natural Sciences and Engineering Research Council (NSERC) Discovery Grant to Hubbard. Data for the NAYS2D numerical model was provided by W. van de Lageweg. Discussions with Dale Leckie, William Matthews, and Fran Hein helped to shape the ideas presented herein. This manuscript was improved by thoughtful comments from *GSA Bulletin* reviewers R. Jacobson and G. Weissman, and Associate Editor J. Florsheim. Their efforts are greatly appreciated. Thanks go to the University of Calgary for providing student funding to Durkin.

REFERENCES CITED

Bailey, R.J., and Smith, D.G., 2005, Quantitative evidence for the fractal nature of the stratigraphic record: Results and implications: Proceedings of the Geologists' Association, v. 116, p. 129–138, https://doi.org/10.1016/S0016-7878(05)80004-5.

Bailey, R.J., and Smith, D.G., 2010, Scaling in stratigraphic data series: Implications for practical stratigraphy: First Break, v. 28, p. 57–66, https://doi.org/10.3997/1365-2397.2010001.

Barrell, J., 1917, Rhythms and the measurements of geologic time: Geological Society of America Bulletin, v. 28, p. 745–904, https://doi.org/10.1130/GSAB-28-745.

Benyon, C., Leier, A., Leckie, D.A., Webb, A., Hubbard, S.M., and Gehrels, G., 2014, Provenance of the Cretaceous Athabasca oil sands, Canada: Implications for continental-scale sediment transport: Journal of Sedimentary Research, v. 84, p. 136–143, https://doi.org/10.2110/jsr.2014.16.

Blum, M., and Pecha, M., 2014, Mid-Cretaceous to Paleocene North American drainage reorganization from detrital zircons: Geology, v. 42, p. 607–610, https://doi.org/10.1130/G35513.1.

Blum, M., Martin, J., Milliken, K., and Garvin, M., 2013, Paleovalley systems: Insights from Quaternary analogs and experiments: Earth-Science Reviews, v. 116, p. 128–169, https://doi.org/10.1016/j.earscirev.2012.09.003.

Brekke, H., MacEachern, J.A., Roenitz, T., and Dashtgard, S.E., 2017, The use of microresistivity image logs for facies interpretations: An example in point-bar deposits of the McMurray Formation, Alberta, Canada: American Association of Petroleum Geologists Bulletin, v. 101, no. 5, p. 655–682, https://doi.org/10.1306/08241616014.

Brice, J.C., 1974, Evolution of meander loops: Geological Society of America Bulletin, v. 85, p. 581–586, https://doi.org/10.1130/0016-7606(1974)85<581:EOML>2.0.CO;2.

Diaz-Molina, M., 1993, Geometry and lateral accretion patterns in meander loops: Examples from the Upper Oligocene–Lower Miocene, Loranca Basin, Spain, *in* Marzo, M., and Puigdefabregas, P., eds., Alluvial Sedimentation: International Association of Sedimentologists Special Publication 17, p. 115–131, https://doi.org/10.1002/9781444303995.ch10.

Durkin, P.R., Hubbard, S.M., Boyd, R.L., and Leckie, D.A., 2015, Stratigraphic expression of intra-point bar erosion and rotation: Journal of Sedimentary Research, v. 85, p. 1238–1257, https://doi.org/10.2110/jsr.2015.78.

Durkin, P.R., Boyd, R.L., Hubbard, S.M., Shultz, A.W., and Blum, M., 2017, Three-dimensional reconstruction of meander-belt evolution, Cretaceous McMurray Formation, Alberta Foreland Basin, Canada: Journal of Sedimentary Research, v. 87, p. 1075–1099, http://dx.doi.org/10.2110/jsr.2017.59.

Fernandes, A.M., Törnqvist, T.E., Straub, K.M., and Mohrig, D., 2016, Connecting the backwater hydraulics of coastal rivers to fluvio-deltaic sedimentology and stratigraphy: Geology, v. 44, p. 979–982, https://doi.org/10.1130/G37965.1.

Fisk, H.N., 1944, Geological Investigation of the Alluvial Valley of the Lower Mississippi River: Vicksburg, Mississippi, U.S. Army Corps of Engineers Mississippi River Commission, 78 p.

Fuller, I.C., 2008, Geomorphic impacts of a 100-year flood: Kiwitea Stream, Manawatu catchment, New Zealand: Geomorphology, v. 98, p. 84–95, https://doi.org/10.1016/j.geomorph.2007.02.026.

Fustic, M., Hubbard, S.M., Spencer, R., Smith, D.G., Leckie, D.A., Bennett, B., and Larter, S., 2012, Recognition of down-valley translation in tidally influenced meandering fluvial deposits, Athabasca oil sands (Cretaceous), Alberta, Canada: Marine and Petroleum Geology, v. 29, p. 219–232, https://doi.org/10.1016/j.marpetgeo.2011.08.004.

Hart, B.S., 2013, Whither seismic stratigraphy: Interpretation, v. 1, p. SA3–SA20, http://dx.doi.org/10.1190/INT-2013-0049.1.

Holbrook, J., 2001, Origin, genetic interrelationships, and stratigraphy over the continuum of fluvial channel-form bounding surfaces: An illustration from middle Cretaceous strata, southeastern Colorado: Sedimentary Geology, v. 144, p. 179–222, https://doi.org/10.1016/S0037-0738(01)00118-X.

Holbrook, J., Whitney, J.A., Rittenour, T.M., Marshak, S., and Goble, R.J., 2006, Stratigraphic evidence for millennial-scale temporal clustering of earthquakes on a continental-interior fault: Holocene Mississippi River floodplain deposits, New Madrid seismic zone, USA: Tectonophysics, v. 420, p. 431–454, https://doi.org/10.1016/j.tecto.2006.04.002.

Hubbard, S.M., Smith, G.D., Nielsen, H., Leckie, A.D., Fustic, M., Spencer, J.R., and Bloom, L., 2011, Seismic geomorphology and sedimentology of a tidally influenced river deposit, Lower Cretaceous Athabasca oil sands, Alberta, Canada: American Association of Petroleum Geologists Bulletin, v. 95, p. 1123–1145, https://doi.org/10.1306/12131010111.

Hudson, P.F., and Kesel, R.H., 2000, Channel migration and meander-bend curvature in the lower Mississippi River prior to major human modification: Geology, v. 28, p. 531–534, https://doi.org/10.1130/0091-7613(2000)28<531:CMAMCI>2.0.CO;2.

Jobe, Z.R., Howes, N.C., and Auchter, N.C., 2016, Comparing submarine and fluvial channel kinematics: Implications for stratigraphic architecture: Geology, v. 44, p. 931–934, https://doi.org/10.1130/G38158.1.

Kemp, D.B., Eichenseer, K., and Kiessling, W., 2015, Maximum rates of climate change are systematically underestimated in the geological record: Nature Communications, v. 6, p. 8890, https://doi.org/10.1038/ncomms9890.

Kleinhans, M.G., and van den Berg, J.H., 2011, River channel and bar patterns explained and predicted by an empirical and a physics-based method: Earth Surface Processes and Landforms, v. 36, p. 721–738, https://doi.org/10.1002/esp.2090.

Labrecque, P.A., Hubbard, S.M., Jensen, J.L., and Nielsen, H., 2011, Sedimentology and stratigraphic architecture of a point bar deposit, Lower Cretaceous McMurray Formation, Alberta, Canada: Bulletin of Canadian Petroleum Geology, v. 59, p. 147–171, https://doi.org/10.2113/gscpgbull.59.2.147.

Leopold, L.B., and Wolman, M.G., 1960, River meanders: Geological Society of America Bulletin, v. 71, p. 769–793, https://doi.org/10.1130/0016-7606(1960)71[769:RM]2.0.CO;2.

Lewin, J., and Macklin, M.G., 2003, Preservation potential for late Quaternary river alluvium: Journal of Quaternary Science, v. 18, p. 107–120, https://doi.org/10.1002/jqs.738.

Lowenstein, T.K., Hein, M.C., Bobst, A.L., Jordan, T.E., Ku, T.L., and Luo, S., 2003, An assessment of stratigraphic completeness in climate-sensitive closed-basin lake sediments: Salar de Atacama, Chile: Journal of Sedimentary Research, v. 73, p. 91–104, https://doi.org/10.1306/061002730091.

Macklin, M.G., Benito, G., Gregory, K.J., Johnstone, E., Lewin, J., Michczynska, D.J., Soja, R., Starkel, L., and Thorndycraft, V.R., 2006, Past hydrological events reflected in the Holocene fluvial record of Europe: Catena, v. 66, p. 145–154, https://doi.org/10.1016/j.catena.2005.07.015.

Mahon, R.C., Shaw, J.B., Barnhart, K.R., Hobley, D.E.J., and McElroy, B., 2015, Quantifying the stratigraphic completeness of delta shoreline trajectories: Journal of Geophysical Research–Earth Surface, v. 120, p. 799–817, https://doi.org/10.1002/2014JF003298.

Miall, A.D., 1985, Architectural-element analysis: A new method of facies analysis applied to fluvial deposits: Earth-Science Reviews, v. 22, p. 261–308, https://doi.org/10.1016/0012-8252(85)90001-7.

Miall, A.D., 2010, Time in sequence stratigraphy, *in* Miall, A.D., The Geology of Stratigraphic Sequences: Berlin, Springer, p. 381–389, https://doi.org/10.1007/978-3-642-05027-5_13.

Miall, A.D., 2014a, Updating uniformitarianism: Stratigraphy as just a set of "frozen accidents," *in* Smith, D.G., Bailer, R.J., Burgess, P.M., and Fraser, A.J., eds., Strata and Time: Probing the Gaps in Our Understanding: Geological Society, London, Special Publication 404, p. 11–36, https://doi.org/10.1144/SP404.4

Miall, A.D., 2014b, The emptiness of the stratigraphic record: A preliminary evaluation of missing time in the Mesaverde Group, Book Cliffs, Utah: Journal of Sedimentary Research, v. 84, p. 457–469, https://doi.org/10.2110/jsr.2014.40.

Moody, J.A., and Meade, R.H., 2014, Ontogeny of point bars on a river in a cold semi-arid climate: Geological Society of America Bulletin, v. 126, p. 1301–1316, https://doi.org/10.1130/B30992.1.

Musial, G., Reynaud, J.Y., Gingras, M.K., Fenies, H., Labourdette, R., and Parize, O., 2012, Subsurface and outcrop characterization of large tidally influenced point bars of the Cretaceous McMurray Formation (Alberta, Canada): Sedimentary Geology, v. 279, p. 156–172, https://doi.org/10.1016/j.sedgeo.2011.04.020.

Muwais, W., and Smith, D.G., 1990, Types of channel-fills interpreted from dipmeter logs in the McMurray Formation, Northeast Alberta: Bulletin of Canadian Petroleum Geology, v. 38, p. 53–63.

Nardin, T.R., Feldman, H.R., and Carter, B.J., 2013, Stratigraphic architecture of a large-scale point-bar complex in the McMurray Formation: Syncrude's Mildred Lake Mine, Alberta, Canada, *in* Hein, F.J., Lecke, D., Larter, S., and Suter, J.R., eds., Heavy-Oil and Oil-Sand Petroleum Systems in Alberta and Beyond: American Association of Petroleum Geologists, Studies in Geology 64, p. 273–311.

Perruca, E., Camporeale, C., and Ridolfi, L., 2007, Significance of the riparian vegetation dynamics on meandering river morphodynamics: Water Resources Research, v. 43, W03430, https://doi.org/10.1029/2006WR005234.

Plotnick, R., 1986, A fractal model for the distribution of stratigraphic hiatuses: The Journal of Geology, v. 94, p. 885–890, https://doi.org/10.1086/629094.

Prokoph, A., and Agterberg, F.P., 1999, Detection of sedimentary cyclicity and stratigraphic completeness by wavelet analysis: An application to late Albian cyclostratigraphy of the Western Canada sedimentary basin: Journal of Sedimentary Research, v. 69, p. 862–875, doi: 1073–130X/99/069–862/$03.00.

Reesink, A.J.H., van den Berg, J.H., Parsons, D.R., Amsler, M.L., Best, J.L., Hardy, R.J., Orfeo, O., and Szupiany, R.N., 2015, Extremes in dune preservation: Controls on the completeness of fluvial deposits: Earth-Science Reviews, v. 150, p. 652–665, https://doi.org/10.1016/j.earscirev.2015.09.008.

Sadler, P.M., 1981, Sediment accumulation rates and the completeness of stratigraphic sections: The Journal of Geology, v. 89, p. 569–584, https://doi.org/10.1086/628623.

Sadler, P.M., 1999, The influence of hiatuses on sediment accumulation rates: GeoResearch Forum, v. 5, p. 15–40.

Sadler, P.M., and Jerolmack, D.J., 2014, Scaling laws for aggradation, denudation and progradation rates: The case for time-scale invariance at sediment sources and sinks, *in* Smith, D.G., Bailer, R.J., Burgess, P.M,. and Fraser, A.J., eds., Strata and Time: Probing the Gaps in Our Understanding: Geological Society, London, Special Publication 404, p. 69–88, https://doi.org/10.1144/SP404.7.

Sadler, P.M., and Strauss, D., 1990, Estimation of completeness of stratigraphical sections using empirical data and theoretical models: Journal of the Geological Society [London], v. 147, p. 471–485, https://doi.org/10.1144/gsjgs.147.3.0471.

Saucier, R.T., 1994, Geomorphology and Quaternary Geologic History of the Lower Mississippi Valley: Vicksburg, Mississippi, U.S. Army Corps of Engineers, Mississippi River Commission, 364 p.

Schlager, W., 2004, Fractal nature of stratigraphic sequences: Geology, v. 32, p. 185–188, https://doi.org/10.1130/G20253.1.

Schumer, R., and Jerolmack, D.J., 2009, Real and apparent changes in sediment deposition rates through time: Journal of Geophysical Research, v. 114, F00A06, https://doi.org/10.1029/2009JF001266.

Smith, D.G., Hubbard, S., Leckie, D., and Fustic, M., 2009, Counter point bar deposits: lithofacies and reservoir significance in the meandering modern Peace River and ancient McMurray Formation, Alberta, Canada: Sedimentology, v. 56, p. 1655–1669, https://doi.org/10.1111/j.1365-3091.2009.01050.x.

Smith, D.G., Bailey, R.J., Burgess, P.M., and Fraser, A.J., 2015, Strata and time: Probing the gaps in our understanding, *in* Smith, D.G., Bailey, R.J., Burgess, P.M., and Fraser, A.J., eds., Strata and Time: Probing the Gaps in our Understanding: Geological Society, London, Special Publication 404, p. 1–10, https://doi.org/10.1144/SP404.16.

Sommerfield, C.K., 2006, On sediment accumulation rates and stratigraphic completeness: Lessons from Holo-

cene ocean margins: Continental Shelf Research, v. 26, p. 2225–2240, https://doi.org/10.1016/j.csr.2006.07.015.

Stouthamer, E., and Berendsen, H.J.A., 2000, Factors controlling the Holocene avulsion history of the Rhine-Meuse Delta (The Netherlands): Journal of Sedimentary Research, v. 70, p. 1051–1064, https://doi.org/10.1306/033000701051.

Straub, K.M., and Esposito, C.R., 2013, Influence of water and sediment supply on the stratigraphic record of alluvial fans and deltas: Process controls on stratigraphic completeness: Journal of Geophysical Research–Earth Surface, v. 118, p. 625–637, https://doi.org/10.1002/jgrf.20061.

Straub, K.M., Paola, C., Mohrig, D., Wolinsky, M.A., and George, T., 2009, Compensational stacking of channelized sedimentary deposits: Journal of Sedimentary Research, v. 79, p. 673–688, https://doi.org/1527-1404/09/079-673/$03.00.

Strauss, D., and Sadler, P.M., 1989, Stochastic models for the completeness of stratigraphic sections: Mathematical Geosciences, v. 21, p. 37–59, https://doi.org/10.1007/BF00897239.

Syvitski, J.P., and Brakenridge, G.R., 2013, Causation and avoidance of catastrophic flooding along the Indus River, Pakistan: GSA Today, v. 23, no. 1, p. 4–10, https://doi.org/10.1130/GSATG165A.1.

Toonen, W.H.J., Kleinhans, M.G., and Cohen, K.M., 2012, Sedimentary architecture of abandoned channel fills: Earth Surface Processes and Landforms, v. 37, p. 459–472, https://doi.org/10.1002/esp.3189.

Trabucho-Alexandre, J., 2014, More gaps than shale: Erosion of mud and its effect on preserved geochemical and palaeobiological signals, *in* Smith, D.G., Bailer, R.J., Burgess, P.M., and Fraser, A.J., eds., Strata and Time: Probing the Gaps in Our Understanding: Geological Society, London, Special Publication 404, p. 251–270, https://doi.org/10.1144/SP404.10.

van de Lageweg, W.I., Schuurman, F., Cohen, K.M., van Dijk, W.M., Shimizu, Y., and Kleinhans, M.G., 2016, Preservation of meandering river channels in uniformly aggrading channel belts: Sedimentology, v. 63, p. 586–608, https://doi.org/10.111/sed.12229.

Wetzel, A., and Aigner, T., 1986, Stratigraphic completeness: Tiered trace fossils provide a measuring stick: Geology, v. 14, p. 234–237, https://doi.org/10.1130/0091-7613(1986)14<234:SCTTFP>2.0.CO;2.

Wheeler, H.E., 1958, Time stratigraphy: American Association of Petroleum Geologists Bulletin, v. 42, p. 1047–1063.

Science Editor: Aaron J. Cavosie
Associate Editor: Joan Florsheim

Manuscript Received 7 November 2016
Revised Manuscript Received 6 August 2017
Manuscript Accepted 8 November 2017

Printed in the USA